International Journal of Hydrogen Energy 85 (2024) 539–559

Contents lists available at ScienceDirect

International Journal of Hydrogen Energy

journal homepage: www.elsevier.com/locate/he

Electricity supply configurations for green hydrogen hubs: A European case study on decarbonizing urban transport

Kamaldeen Adekola [a,*], Samim Ghafoori [b], François Dechamp [b], Alessandro Prada [c]

[a] Delft University of Technology, Faculty of Technology, Policy, and Management, Delft, the Netherlands
[b] Research and Development Unit, ABMI Engineering Company, Nanterre, France
[c] Department of Civil, Environmental and Mechanical Engineering, University of Trento, Trento, Italy

ARTICLE INFO

Handling Editor: Prof. J. W. Sheffield

Keywords:
Integrated energy systems
Green hydrogen hub
Hydrogen bus
Fleet decarbonization
Renewable energy systems

ABSTRACT

In this study, a techno-economic analysis tool for conducting detailed feasibility studies on the deployment of green hydrogen hubs for fuel cell bus fleets is developed. The study evaluates and compares five green hydrogen hub configurations' operational and economic performance under a typical metropolitan bus fleet refuelling schedule. Each configuration differs based on its electricity sourcing characteristics such as the mix of energy sources, capacity sizing, financial structure, and grid interaction. A detailed comparative analysis of distinct green hydrogen hub configurations for decarbonising a fleet of fuel-cell buses is conducted. Among the key findings is that a hybrid renewable electricity source and hydrogen storage are essential for cost-optimal operation across all configurations. Furthermore, bi-directional grid-interactive configurations are the most cost-efficient and can benefit the electricity grid by flattening the duck curve. Lastly, the paper highlights the potential for cost reduction when the fleet refuelling schedule is co-optimized with the green hydrogen hub electricity supply configuration.

1. Introduction

From 1990 to 2020, reductions in CO_2 emissions have been achieved in the European Union (EU) across key sectors such as public electricity production, manufacturing, industrial, chemical, and residential. However, the same progress has not been observed in the road transportation sector, which has instead experienced a continued increase in CO_2 emissions [1]. Nicole and Marion [1] estimate an increase of 52.7 Mt of CO_2 emissions in transport compared to reductions of 59.3 Mt in residential and 357 Mt in manufacturing sectors. The transport sector's reliance on oil as its primary fuel source has contributed to its substantial and growing contribution to greenhouse gas emissions [2]. In 2020, road transportation accounted for 26% of total CO_2 emissions and is projected to account for the largest share of CO_2 emissions by 2050 in the absence of ambitious steps towards decarbonization [1,3]. This is due to the estimated growth in demand for passenger and freight transport by 40% and 60% respectively between 2010 and 2050 [3].

In response to this, the European Commission has proposed a target of zero emissions for new city buses by 2030 [4]. To achieve this, it may be necessary for cities to adopt all-electric vehicles in the form of either battery electric vehicles (BEV) or hydrogen fuel cell electric vehicles (FCEV), for their city buses. Both BEVs and FCEVs have the potential to reduce CO_2 emissions and air pollution from road transport since they produce the minimum well-to-wheel emissions and no harmful tank-to-wheel emissions such as nitrogen oxides, particulate matter, and sulfur dioxide [5]. When compared, both have their advantages over the other, as well as drawbacks. Several studies comparing the technical, economic, and environmental performance of BEVs, FCEVs and other alternative fuel vehicles exist in the literature. However, this study does not focus on the comparison between various alternative fuel vehicles. For this, readers are referred to Refs. [5–8].

This paper describes, analyzes, and compares distinct energy supply configurations for an on-site green hydrogen production hub for refuelling a fleet of FCEV buses. A major barrier to the broader adoption of FCEVs is the lack of green hydrogen production infrastructure [9–11]. In their qualitative study, Axsen and Pickrell-Barr [10] identify the scarcity of refuelling infrastructure as the most stated barrier to the adoption of alternative fuel vehicles by organizations for their transport fleets. The International Energy Agency IEA notes that the transport sector, through fleets, is one of the key near-term opportunities to accelerate green

* Corresponding author.
E-mail addresses: k.k.adekola@tudelft.nl (K. Adekola), m.ghafoori@abmi-groupe.com (S. Ghafoori), f.dechamp@abmi-groupe.com (F. Dechamp), alessandro.prada@unitn.it (A. Prada).

https://doi.org/10.1016/j.ijhydene.2024.08.336
Received 10 June 2024; Received in revised form 17 August 2024; Accepted 20 August 2024
Available online 26 August 2024

hydrogen adoption [12]. Public bus fleets particularly, have the potential to catalyze expansion of green hydrogen infrastructure due to their central operation as well as large and predictable fuel demand. Moreover, green hydrogen has the potential to serve as an energy vector that connects the transport and power sectors, for example, by flattening the duck curve. Thus, the use of FCEVs has significant benefits for the energy transition even beyond transport sector decarbonization. As such, it is topical to explore green hydrogen production strategies for public bus fleets refuelling. Moreover, since electricity constitutes the major cost in electrolytic hydrogen production [13], this paper focuses on studying various electricity supply configurations for the aforementioned application.

The objectives of this paper include the modelling, analysis, and comparison of the techno-economic performance of a green hydrogen hub designed to supply hydrogen to a fuel cell bus fleet, such as a public transport company with a rigid demand schedule under various electricity sourcing arrangements. Section 2 discusses relevant literature on green hydrogen production with a focus on transport decarbonization. Section 3 presents the case study and the computational framework for the study. Section 4 describes the modelling of the green hydrogen hub and the various configurations analyzed in this work. In Section 5, we respectively present the result and discuss the key insights obtained. We provide the conclusion of the study and future work in Section 6.

2. Review of literature

Several methods exist for producing hydrogen from renewable sources including thermochemical, electrochemical, photochemical, photocatalytic, and photo-electrochemical processes [14]. However, according to the International Renewable Energy Agency (IRENA), the term green hydrogen refers only to hydrogen produced with electricity from renewable sources [15]. Thus, the green hydrogen value chain typically describes the production, storage, and distribution of hydrogen that is generated from renewable energy sources [16]. In academic literature, wind energy is a popular choice for green hydrogen production due to its scalability, reliability, and low operating costs [17–20]. Similarly, photovoltaic (PV) systems have also been demonstrated as a feasible renewable energy resource for green hydrogen production [21,22]. Other renewable sources such as hydroelectric power, geothermal energy, and biomass can also be used to generate electricity for green hydrogen production [12].

In [23], the term “green hydrogen hub” refers to the entire value chain of electrolytic hydrogen production, including storage and distribution to end-users. “Hydrogen refuelling station” (HRS), on the other hand, is defined as an infrastructure deployed for refuelling FCEVs [11]. In this work, we use both terms loosely as the study focuses on the entire hydrogen value chain, with a particular focus on transport application. HRS can be classified as either on-site or off-site, depending on the location of hydrogen production [11]. In off-site HRS, hydrogen is produced elsewhere and transported to the HRS whereas in on-site HRS, the hydrogen production takes place directly at the location of the hydrogen demand [11]. Due to the focus of this study, we consider only on-site HRS. The core components of an on-site green hydrogen refuelling station include the renewable electricity source, electrolyser, compressor, hydrogen storage (including buffer Storage and high-pressure storage), hydrogen dispenser and balance of plant. In this study, the balance of plant refers to any device that enables the electrolyser to function but is not explicitly modelled, such as water tanks, water purifiers, hydrogen purifiers, transformers, pumps, etc., since their power consumption is not significant for this study. Below, we provide a brief overview of the core components found in HRS.

The minimum energy required by an electrolyser operating at 100% efficiency is 39.4 kWh per kg of hydrogen (or 0.03 kgH_2/kWh), but typical electrolysers consume over 50 kWh/kg [14]. Since the electrolyser efficiency varies with a range of factors, the average electrolyser efficiency for this study is taken as 64% for a continuous operation of PEM electrolyser as suggested in Ref. [24], resulting in a specific energy consumption of 62 kWh/kgH_2. The method for the calculation of the specific energy consumption of an electrolyser is provided in Ref. [25]. Furthermore, state-of-the-art PEM electrolysers can operate with the high flexibility and responsiveness needed for intermittent renewable energy-powered electrolysis [26,27], as such, we assume PEM electrolyser in our cost and technical assumptions.

Hydrogen gas is typically stored at pressures ranging from 350 to 700 bar, requiring compression to achieve the energy density necessary for most practical applications, including transport [28]. Although, other forms of storage exist such as liquefied hydrogen [29] and storage in materials such as metal hydrides, Mg-based alloys, carbon-based materials, chemical hydrides, and boron compounds [30,31], they have not gained widespread adoption in HRS or FCEV applications. Therefore, for this study, compressed gas storage is utilized. The hydrogen compression and storage system consists of a low-pressure 30-bar buffer storage that holds hydrogen exiting the PEM electrolyser temporarily before it is sent into the compressor which compresses it to 500 bar and is stored in a high-pressure hydrogen storage tank [28]. The French Environment and Energy Management Agency (ADEME) recommends compressing up to 500 bar for 350 bar applications and up to 900 bar for 700 bar applications [32]. We adopt the method in Ref. [33] to calculate the compressor power and specific energy consumption.

The hydrogen dispensing unit consists of two main components: the refrigeration system and the dispenser nozzle. The refrigeration system ensures that the hydrogen is kept at a certain temperature range as specified by the SAE J2601 fueling protocol while the dispenser nozzle regulates the gas flow [34]. SAE J2601 which provides the requirements for fueling 350 bar hydrogen buses stipulates that the delivery temperature of the hydrogen should not be less than −40 °C or greater than −17.5 °C during the fueling process [35]. This is to account for the negative Joule-Thompson coefficient of hydrogen, which refers to the phenomenon where the temperature of gases increases as it expands. To prevent a temperature increase that could be dangerous for the hydrogen tank in the FCEVs, the hydrogen needs to be precooled before fueling. The power requirement for the refrigeration system can be calculated using the approach in Ref. [22]. However, we neglect the energy consumption of the hydrogen dispensing unit since it is insignificant when compared to that of the electrolyser and the compressor [22].

Various strategies have been used in literature to meet the energy requirements of green hydrogen hubs. A common strategy is the direct connection of a green hydrogen hub with a dedicated off-grid renewable energy infrastructure used in Refs. [36–39]. Alternatively, hydrogen hubs can be connected to the grid (coupled with renewable energy guarantees), participating in the electricity market [40–42]. Lastly, a hybrid solution where the green hydrogen hub is connected with a grid-interactive renewable energy infrastructure is also a common strategy [43–45]. Some studies have also compared the use of off-grid and grid-interactive approaches, where the on-grid strategy is shown to lead to a lower levelized cost of hydrogen (LCOH) [46,47]. However, they do not consider alternative electricity cost structures such as Power Purchase Agreements (PPAs).

The electricity cost structure for green hydrogen production can range from annualized investment cost to alternative cost structures such as a Power Purchase Agreement (PPA) with an existing renewable energy supplier as presented by Matute et al. in Ref. [48]. While PPAs are often flexibly structured and tailored to the specific needs of the buyer, the basic idea behind renewable PPAs is the commitment from a buyer to acquire future electricity output from a renewable energy producer at a pre-established fixed price [49]. They offer a promising strategy for generating green hydrogen from renewable energy without incurring significant capital costs from renewable energy infrastructure development [48]. In the remaining part of this section, we highlight some recent academic work on green hydrogen production in on-site HRS with a particular focus on hydrogen bus fleets.

Minutillo et al. [22] conducted a techno-economic analysis of an on-site hydrogen refuelling station, integrating an electrolysis unit with a grid-connected PV plant in southern Italy. Their study assessed the LCOH across a range of electricity supply scenarios by varying the electricity supply mix and hydrogen production capacities. The range of LCOH obtained was between 9.29 €/kg and 12.48 €/kg using an annualized investment cost structure for the PV plant. However, the study did not focus on bus fleet decarbonization with an inflexible hydrogen demand profile. Gökçek et al. [50] studied the optimal design of a hydrogen refuelling station on an island in Türkiye using Homer software. The result indicates an optimal LCOH at $8.92/kg with a hybrid wind-photovoltaic battery system, using an off-grid configuration. They further expand the study to more cities and additional electricity supply scenarios [51]. In Ref. [52], Oyewole et al. present an integrated energy system that combines hydrogen renewable power generation and an onsite HRS using data for Johannesburg. A feasibility study is conducted to evaluate the potential of the system to meet both electricity and hydrogen demands under three distinct configurations: hybrid PV-wind, standalone wind, and standalone PV. The findings suggest that the hybrid PV-Wind configuration is the most cost-effective with an LCOH of $2.83/kg. Although the study mentions the possibility of exporting excess energy to the grid, it does not model a grid-connected configuration. While most studies on HRS and green hydrogen hubs do not focus on fleet decarbonization, a limited number discussed below address this application.

Bahou [43] conducts a techno-economic assessment of a hydrogen refuelling station designed to supply hydrogen to an FCEV taxi fleet in Rabat, Morocco. The HRS utilizes an on-grid photovoltaic solar system as an electricity source. The LCOH ranged from $9.18/kg for a larger HRS designed to meet the total fleet hydrogen demand of 152 kg/day, to $12.56/kg for an HRS designed to meet 20% of the hydrogen demand. Caponi et al. [53] carried out a techno-economic analysis of five HRS focusing on the individual component costs of scaling up the refuelling stations to meet the hydrogen demand of 100 hydrogen-electric buses per day. Their findings also indicate that on-site HRS is more cost-effective than off-site HRS. They also identify the main cost driver of on-site HRS to be the electricity price. Additionally, their study suggests that scaling up HRS can result in significant reductions in LCOH. The LCOH obtained ranged from 4 €/kg to 7 €/kg across the case studies considered. In Ref. [42], an on-site HRS designed to supply hydrogen to a fleet of 2–30 hydrogen-electric buses is presented. The HRS is powered through grid electricity and exposed to wholesale electricity prices. The LCOH for the larger fleet was found to be more cost-effective at 10.2 €/kg compared to 12 €/kg for the smaller fleet. The results indicate that hydrogen bus fleets are not cost-competitive under this configuration due to high electricity prices, especially when compared to battery electric buses. However, the limited range of electricity supply configurations considered inhibits the generalizability of these findings. Coppitters et al. in Ref. [54] study how diesel can be cost-effectively replaced in Brussels using green hydrogen by optimizing the design of an HRS. They modelled an on-site HRS powered by a grid-connected, hybrid renewable electricity source consisting of wind and PV. The study examined three scenarios: a fully diesel-powered bus fleet, a hybrid fleet of both diesel and hydrogen electric buses, and a fully hydrogen-powered bus fleet. The findings from the study suggest that replacing 54% of the fleet with hydrogen-electric buses strikes an optimal balance between cost and emissions. The study reports an LCOH of 17–18.9 €/kg for the optimal HRS designs. A comprehensive review of the state-of-the-art in green hydrogen for transport applications is provided in Ref. [11].

In summary, energy supply for green hydrogen hubs can be categorized into two: off-grid and grid-connected energy resources. In both energy supply arrangements, studies typically focus on a singular renewable energy source, usually wind or PV. However, some studies also investigate hybrid renewable energy system configurations consisting of both PV and wind in either off-grid or grid-connected mode. Furthermore, the common cost structure utilized for electricity supply is the annualized investment cost, while grid-connected systems also incorporate wholesale electricity prices. A few studies examine the potential of PPA for green hydrogen hubs. Since most studies focus on one of these approaches, without explicit analysis of the optimal electricity supply arrangement, we perform a comparative analysis of the commonly used electricity supply configurations for green hydrogen hubs. Considering the significance of electricity cost in electrolytic hydrogen production, such analysis is essential. We study five configurations of electricity supply to the green hydrogen hub as follows:

- Direct coupling with standalone renewable energy systems using annualized investment cost.
- Direct coupling with standalone renewable energy systems using PPA.
- Unidirectional grid-connected energy source with carbon pricing.
- Grid-interactive renewable energy system using annualized investment cost.
- Grid-interactive renewable energy system using PPA.

The main contribution of this work is the comparative analysis of different electricity supply configurations to a green hydrogen hub designed for refuelling a fleet of hydrogen electric buses. We consider a use case of public transport decarbonization where buses are typically owned by a central organization such as a public transport company and the fuel demand profile is usually known. The objective of the study is to understand the impact of various electricity supply configurations on the technical and economic performance of a green hydrogen hub. We also conduct a sensitivity analysis to understand the influence of parameters such as location, capital expenditure, electricity costs, and hydrogen demand schedule.

3. Methodology

3.1. Case study

The Cannes Pays de Lérins Agglomeration Community (CPAC) in the Provence-Alpes-Côte d'Azur region of France announced plans to expand the Cannes Lérins H_2 project, focused on using hydrogen-powered buses for passenger transport [55]. The production will be powered by renewable electricity through renewable energy guarantees of origin, and the site will have storage facilities and distribution terminals. The community plans to order fifty-four hydrogen-powered buses and six waste trucks, further expanding the use of green hydrogen in the region. The proposed Cannes Lérins H_2 project forms the primary case study for this research project. Hydrogen hub configurations are designed with the primary objective of meeting the hydrogen requirements of a fully operational fleet of sixty fuel-cell electric vehicles at the least cost of hydrogen. Detailed specifications of technical and cost parameters for the green hydrogen hub are presented in Table 1. This study additionally replicates the Cannes Lérins H_2 project, assuming the same hydrogen needs, across four cities in Spain, Italy, Germany, and Norway. This is to examine the impact of geographical location on the LCOH of such projects. Please refer to Tables 2 and 3 for detailed data.

The minimum daily hydrogen demand to be met includes hydrogen demand for sixty hydrogen electric buses. It is assumed that all the vehicles deployed (N) are 12-m buses with the same hydrogen consumption rate. Data from a previous FCEV study in the Netherlands [56] where 2 hydrogen city buses were deployed to replace the diesel equivalent, the average hydrogen consumption was 7kg/100 km. In this study, the average hydrogen consumption (H_D) is conservatively set at 8.5kg/100 km to consider differences in terrain. An average daily travel distance (D) is estimated to be 300 km including the travel distance to the refuelling station. Equation (1) is used to estimate the daily hydrogen demand for the project. Fig. 1 shows the baseline hourly hydrogen refuelling schedule for a typical day obtained from Equation

Table 1
Parameters used to model the various green hydrogen hub components.

Electrolyser				
Parameter/Unit		Value	Ref	
Lifetime (years)		10	[48]	
Average Efficiency (%)		64	[24]	
Specific Energy Consumption (kWh/kgH_2)		62	calculated	
Output Pressure (bar)		30	[48]	
Upper Capacity Limit (%)		100	[27]	
Lower Capacity Limit (%)		0	[27]	
Hot Start Ramp time (seconds)		2	[27]	
Cold Start Ramp time (seconds)		30	[27]	
	Worst Case	Medium Case	Best Case	Ref
Capex (€/kW)	1758	1005	327	[66]
Replacement Cost (€/kW)	879	502	164	[66]
Fixed Opex (€/kW/year)	43	43	43	[66]

Wind Turbine				
Parameter		Value	Ref	
Nominal power (kW)		3000	[62]	
Model		V126/3000	[62]	
Lifetime (years)		25	[67]	
	Worst Case	Medium Case	Best Case	Ref
Capex (€/kW)	1855	1380	958	[67]
Fixed Opex (€/kW/year)	48	38	28	[67]
Lifetime	25	25	25	[67]
WACC (%)	5	5	5	[67]

PV System				
Parameter		Value	Ref	
Rated capacity (W)		300	[63]	
Model		Silevo_Triex_U300_Black_2014_	[63]	
Lifetime (years)		25	[67]	
	Worst Case	Medium Case	Best Case	Ref
Capex (€/kW)	869	687	590	[67]
Fixed Opex (€/kW/year)	17	12	8	[67]
Lifetime	25	25	590	[67]

Diaphragm Compressor		
Parameter	Value	Ref
Lifetime (years)	10	[48]
Energy Intensity (kWh/kg H_2)	2.62	calculated
Rated Compressor Power (kW)	219	calculated
Inlet Pressure (bar)	20–30	[33]
Outlet Pressure (bar)	500	[33]
Isentropic Efficiency (%)	60	[33]
Motor Efficiency (%)	95	[33]
Compression Ratio per Stage	3.1	[33]
Capex (€/(kg/h))	10000	[68]
Replacement cost (€/(kg/h))	5000	calculated
Fixed Opex (€/kW/year)	800	calculated

Buffer Storage		
Parameter	Value	Ref
Pressure (bar)	30	Assumed
Lifetime (years)	25	[69]
Capex (€/kg)	510	[69]
Fixed Opex (€/kg/year)	2.55	calculated

High-Pressure Storage		
Parameter	Value	Ref
Pressure (bar)	500	Assumed
Lifetime (years)	25	[69]
Capex (€/kg)	1644	[22]
Fixed Opex (€/kg/year)	3	calculated

Hydrogen Dispenser		
Parameter	Value	Ref
Refuelling Station Type	T40 (Precool H_2 to −40 °C)	[70]
Nozzle Flow rate (g/sec)	50	[70]

(continued on next page)

Table 1 (*continued*)

Hydrogen Dispenser		
Parameter	Value	Ref
Refuelling Duration (minutes)	15	calculated
Capex (€/unit)	85000	[28]
Fixed Opex (€/unit/year)	2550	calculated
Lifetime (years)	25	[28]

Battery Energy Storage System		
Parameter	Value	Ref
Capex (€/kW)	850	[12]
Replacement Cost (€/kW)	425	calculated
Fixed Opex (€/kW/year)	8.5	[12]
Lifetime	13	[12]
Round-trip Efficiency	86	[12]

Balance of Plant		
Parameter	Value	Ref
Parameters	Value	Source
Capex (€/kW)	43	[66]
Water (€/kg)	0.07	[66]
Quantity of Water (kg water/kg H2)	20	[15]

Grid Taxes and Levies		
Grid Taxes and Levies (€/kWh/year)	Value	Ref
France	0.025	[57]
Spain	0.005	[57]
Italy	0.065	[57]
Norway	0.012	[71]
Germany	0.070	[57]

Wholesale Electricity Market Bidding Zone		
Country	Bidding Zone	
France	FR	[60]
Spain	ES	[60]
Italy	IT_SUD	[60]
Norway	NO_1	[60]
Germany	DE_LU	[60]

Grid Carbon Intensity		
Grid Carbon Intensity ($kgCO_2e/kWh$)	Value	Ref
France	0.058	[72]
Spain	0.165	[72]
Italy	0.234	[72]
Norway	0.030	[72]
Germany	0.348	[72]

Table 2
Existing wind farm locations considered across 5 European countries.

Country	Latitude	Longitude	City	Region	Ref
France	43.551694	5.798611	Artigues, Ollières	Provence-Alpes-Côte d'Azur	[73]
Spain	37.169833	−3.153555	Málaga	Andalucía	[74]
Italy	42.434665	11.789771	Viterbo	Lazio	[75]
Norway	63.881708	10.16758	Storheia	Trøndelag	[76]
Germany	53.131972	12.122166	Pritzwalk	Brandenburg	[77]

Table 3
Existing PV plant locations considered across 5 European countries.

Country	Lat	Long	City	Region	Ref
France	43.622739	6.753182	Callian	Provence-Alpes-Côte d'Azur	[78]
Spain	37.220888	−4.13205	Seville	Andalucía	[79]
Italy	42.409	11.5717	Montalto di Castro	Lazio	[80]
Norway	63.3444	10.3751	Trondheim	Trøndelag	[81]
Germany	51.544999	13.98	Schipkau	Brandenburg	[82]

(1) by applying the hourly hydrogen refuelling pattern from the New-BusFuel case studies in Ref. [57]. Additionally, an alternative temporal distribution of hydrogen demand represented as the "Daylight Refuelling Schedule" is analyzed to understand the impact of the hydrogen demand pattern on the levelized cost of hydrogen.

$$\textit{Daily Hydrogen Demand}\ (kg) = H_D\ .\ D\ .\ N \qquad \text{Equation 1}$$

The solar radiation and other meteorological data used for solar energy modelling are sourced from the Photovoltaic Geographical Information System's (PVGIS) typical meteorological year (TMY) data set [58], generated following the ISO 15927-4 procedure [21,22]. The wind resource data is fetched from the Application Programming Interface (API) provided by the New European Wind Atlas (NEWA) [59]. Although NEWA presents the data at a temporal resolution of 30 min, it is resampled to an hourly resolution to match the temporal resolution of other datasets used in this study. As NEWA does not offer TMY data, the data for the year 2018, which is the most recent in the database have been used. Wholesale Electricity Market data including the day-ahead electricity prices and load data are extracted from the European Network of Transmission System Operators for Electricity (ENTSO-E) transparency platform through its API [60]. The load data and day-ahead electricity prices are used as input parameters in the

Fig. 1. Hydrogen demand patterns by the metropolitan bus fleet throughout the day.

hydrogen hub configurations that involve grid interactivity. The year 2022 data is used as the baseline scenario across all locations considered.

In this study, the windpowerlib Python library [61] is employed to convert wind resource parameters into the energy output of a wind turbine (*WT*). The specific *WT* model used is the Vestas V126/3000 with a hub height of 100 m. The power curve and power coefficient curve (Fig. 2) for this model were accessed from the open energy platform [62]. Nonetheless, the techno-economic analysis tool developed enables the use of any desired wind turbine provided the power curve and power coefficient curve are provided.

The open-source Python library, pvlib [63] was used for simulating the performance of the PV system module 'Silevo_Triex_U300_-Black_2014_' with a rated capacity of 300W using the input TMY data [64]. The Hay-Davies model was used to transpose irradiance to the tilted plane of the PV modules [63]. Finally, the Sandia Array Performance Model was used to calculate the actual DC power output considering the non-linear changes in power output with varying irradiance levels, temperature-dependent changes in the maximum power point, light-induced degradation, and module aging. The. The solar PV system's specifications were sourced from the System Advisor Model (SAM) [65], a tool developed by the National Renewable Energy Laboratory (NREL).

3.2. Computational framework

The techno-economic analysis tool developed primarily solves a linear optimization problem for a green hydrogen production hub. Depending on the configuration, the hub comprises several components including the PV system, wind turbines, battery energy storage system, PEM electrolyser, a hydrogen compressor, and a hydrogen storage system. The goal of the optimization is to minimize the total cost (capital and operational costs) of hydrogen production given a rigid hydrogen demand schedule as outlined in 2.1 above. The objective function is subject to hydrogen demand constraints and other conditions critical for the appropriate operation of the system. The computational framework illustrated in Fig. 3 initiates with data extraction of hourly wind and irradiance profiles, hourly wholesale energy market data, and the temporal distribution of hydrogen demand throughout the day. Additionally, it encompasses the technical and economic data on each component of the green hydrogen hub.

Subsequently, the optimization problem is formulated and modelled using Pyomo [83,84], a Python-based optimization modelling language. This step involves the definition of suitable variables, parameters, constraints, and a linear objective function. While Gurobi [85] is the primary solver utilized, the techno-economic analysis tool also provides compatibility with GLPK [86]. Following the optimization process, a cost analysis is performed on the solver output, followed by a detailed

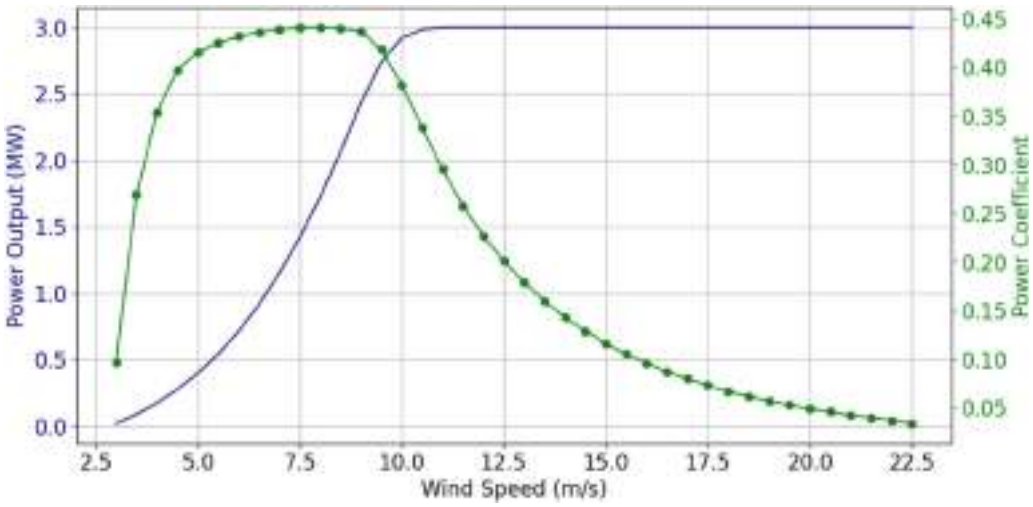

Fig. 2. Power curve and power coefficient curve of vestas v126/3000.

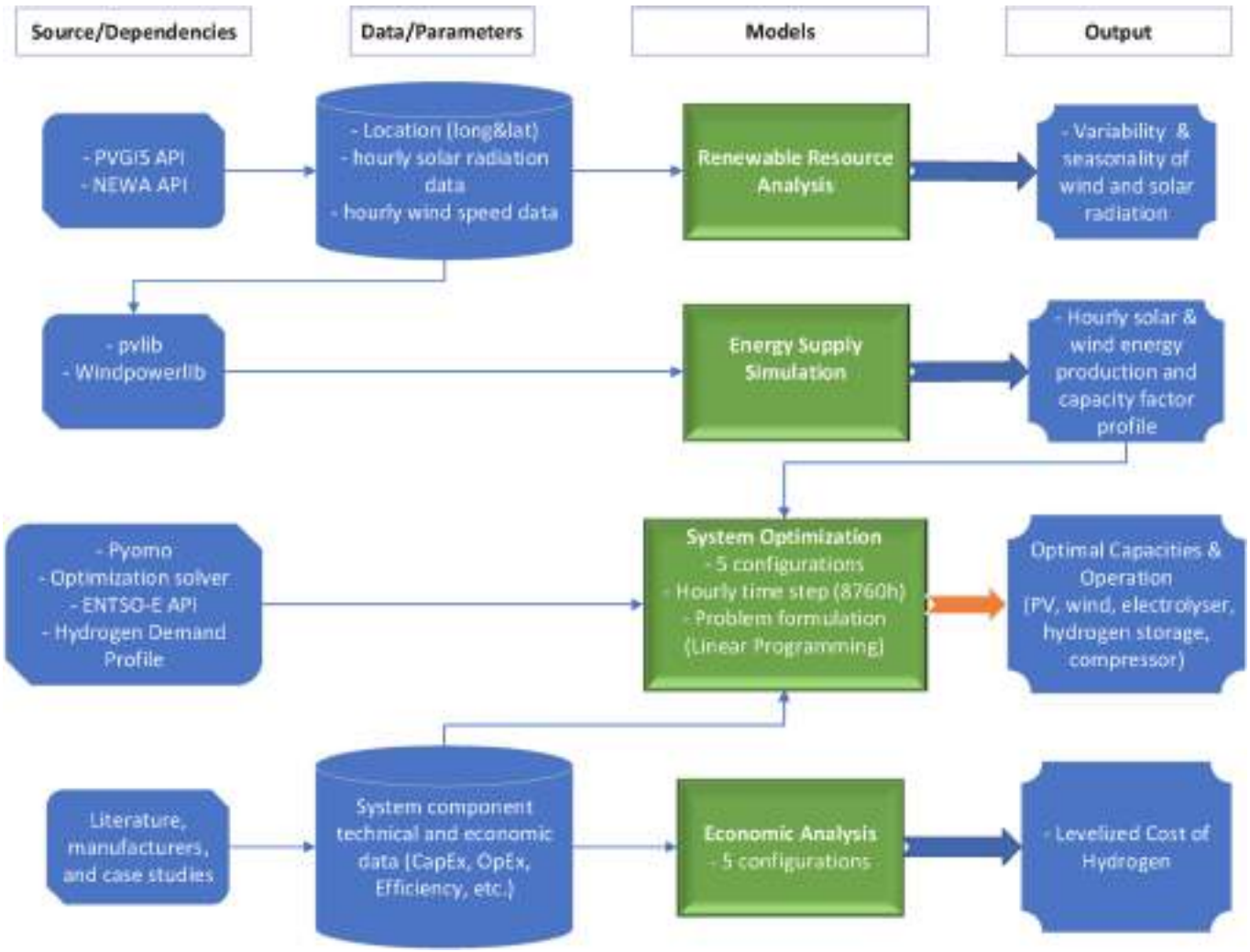

Fig. 3. Green hydrogen hub modelling framework. (For interpretation of the references to colour in this figure legend, the reader is referred to the Web version of this article.)

analysis of the results. The simulation framework considers five different green hydrogen hub configurations, differing from each other in energy supply for hydrogen production.

4. Green hydrogen Hub Modeling

The green hydrogen hub is modelled as a multi-time, constrained optimization problem, and formulated as a Linear Programming problem. The study uses historical data processed with an hourly time step, resulting in a total of 8760 h representing the dynamic behaviour of the system throughout a typical year. The study assumes that the PEM electrolyser can be operated flexibly considering the intermittent supply of electricity. It maintains constant efficiency, ignoring the complex behaviour that might affect electrolyser efficiency and no considerations for degradation or ageing. There is an assumption of perfect foresight regarding the electricity supply from renewable sources and grid electricity prices, however, sensitivity analysis is conducted to determine the impact of variation of these parameters. The carbon intensity of the electricity grid and Power Purchase Agreement (PPA) prices are assumed to be fixed throughout the project's lifetime. The grid interaction constraints are simplified (please refer to Equation (10)), and continuous operation of the green hydrogen hub is anticipated for the entire project duration. The model does factor in the network charges for electricity transmission costs per MWh of electricity consumed but assumes no changes in regulations or policies during the lifespan of the project. Finally, the hydrogen demand profile of urban bus fleets is assumed to be unchanged and inflexible throughout the project lifetime.

4.1. Direct coupling with standalone renewable energy systems

Firstly, a standalone, or 'island mode', renewable energy setup to produce green hydrogen is modelled as illustrated in Fig. 4. We evaluate a standalone system using annualized investment cost for renewables (Configuration 1) and an alternative cost structure, PPA (Configuration 2) further explained below.

4.1.1. Problem formulation - configuration 1

Configuration 1 has dedicated renewable energy plants whose cost structure is annualized investment cost. The renewable energy plants are developed and sized optimally for the green hydrogen hub. As such, the green hydrogen hub can operate independently of third parties, enabling greater control of its energy supply and seamless integration of renewable energy resources and hydrogen production systems. These advantages come at the expense of significantly higher investment costs, exposure to failures of the renewable energy system, responsibility for the maintenance and operation of the renewable energy system, and technology lock-in.

In its problem formulation, the objective is to minimize the total cost (TC) of the green hydrogen hub required to meet the hourly hydrogen demand of the metropolitan fuel cell bus fleet. The objective function is

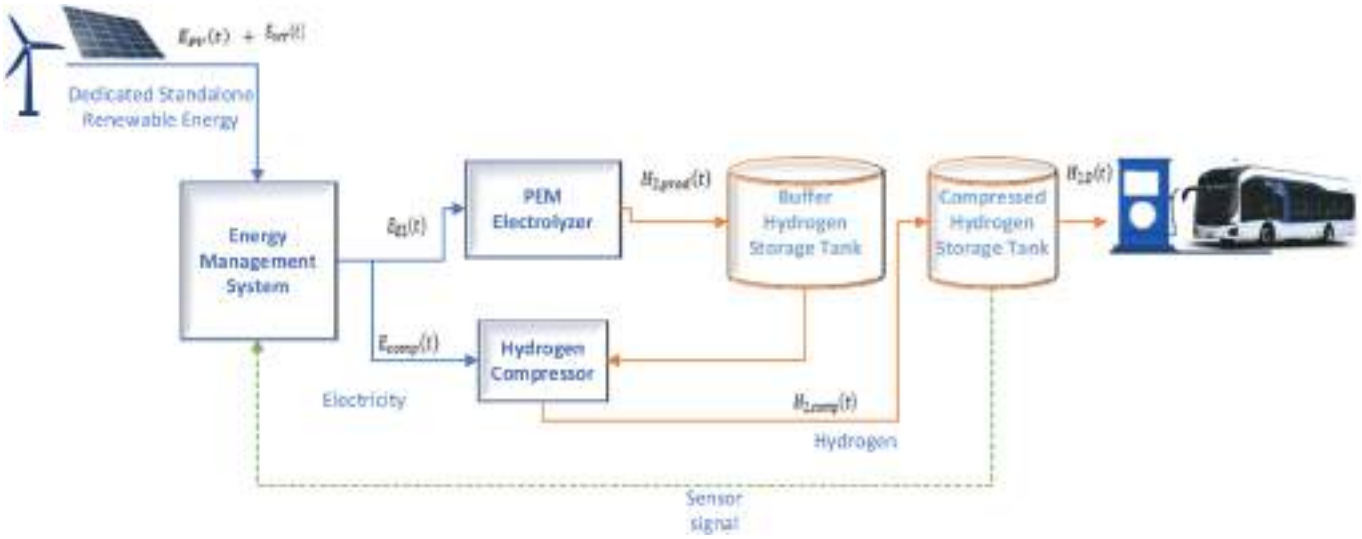

Fig. 4. Schematic representation of Configurations 1 and 2.

formulated in Equation (2).

$$minimize\ TC = \sum_{x\ \epsilon\ X}\left[\left(R_x\ .\ C_{cap,x}\ .\ S_x\right) + \left(C_{op,x}\ .\ S_x\ .N\right)\right] \quad \text{Equation 2}$$

$x \epsilon X$ denotes the set of system components considered and illustrated in the respective schematic configurations.

The optimization is also subject to several constraints. Equation (3) represents the energy balance constraints for configurations 1 and 2. It ensures that the sum of the energy consumed by the electrolyser (E_{EL}), compressor (E_{comp}), and battery charging (B_{ch}) does not surpass the total energy produced by the wind turbines (E_{WT}), battery discharging (B_{dis}) and photovoltaic systems (E_{PV}) at any given time t.

$$\forall t : E_{EL}(t) + E_{comp}(t) + \frac{B_{ch}(t)}{\eta_{ch}} \leq E_{WT}(t) + E_{PV}(t) + \eta_{dis}\ .\ B_{dis}(t) \quad \text{Equation 3}$$

Other constraints that are the same across all the different configurations of the green hydrogen hub such as capacity constraints, hydrogen storage constraints, compressor operation and battery storage constraints are detailed in the appendix section A.

4.1.2. Problem formulation - configuration 2

Configuration 2 operates under a mechanism known as a physical Power Purchase Agreement (PPA). In this PPA setup, renewable electricity is bought 'as produced' from a third-party renewable energy producer. As-produced PPAs are long-term agreements in which the energy producer manages the maintenance and operation of the energy production system. In return, the green hydrogen hub contractually commits to buying the generated power at a predetermined price throughout the agreed period. This offers long-term electricity cost predictability and stability. The PPA arrangement provides a more flexible way of accessing renewable energy without needing to directly own or manage the resources. However, the renewable energy system sizing is not typically optimized for demand and may suffer from electricity supply inadequacy or oversizing.

The main difference in problem formulation lies in the calculation of electricity costs from wind and photovoltaic resources. Unlike Configuration 1, where the installation costs for PV and wind technologies are treated as annualized capital expenditures, they are regarded as fixed operational expenditures in Configuration 2, in the form of a PPA with renewable energy suppliers. Here, the sizing of wind farms and solar PV systems is predetermined and not included as optimization variables.

The objective function for configuration 2 is presented in Equation (4), where the total cost is minimized by taking into account the renewable energy consumed and its respective fixed price under the power purchase agreements together with other costs (i.e. electrolyser, compressed and hydrogen buffer storage, compressor, balance of plant and battery energy storage). All the constraints used in Configuration 1 similarly apply to Configuration 2.

$$minimize\ TC = N\ .\ \sum_{t=1}^{T}\left(\ E_{WT}(t)\ .\ PPA_{wind} + E_{PV}(t)\ .\ \ PPA_{solar}\right) + \sum_{x\ \epsilon\ X}\left[\left(R_x\ .\ \ C_{cap,x}\ .\ S_x\right) + \left(C_{op,x}\ .\ S_x\ .N\right)\right] \quad \text{Equation 4}$$

4.2. Unidirectional grid-connected energy source with carbon pricing

In this scenario (Configuration 3), the primary source of electricity for the green hydrogen hub is the electricity grid (Fig. 5), removing the need for substantial investments in renewable energy infrastructure or long-term contracts with energy suppliers. The production of green hydrogen is enabled by electricity from the grid purchased through the wholesale electricity market. Additional costs due to carbon pricing are incurred. The main challenge is the volatility of the wholesale electricity market, which could lead to decreased predictability and stability in costs.

4.2.1. Problem formulation - configuration 3

The objective function aims to minimize the total costs (TC), which include the cost of electricity from grid consumption and the capital and fixed operating costs associated with the infrastructure installed. This is mathematically expressed in Equation (5) below.

$$minimize\ TC = N\ .\ \sum_{t=1}^{T}\left(E_{Grid,buy}(t).\left(p_{Grid}(t) + F_{Grid} + I_{CO2}\ .\ \ C_{CO2}\right)\right) + \sum_{x\ \epsilon\ X}\left[\left(R_x\ .\ \ C_{cap,x}\ .\ S_x\right) + \left(C_{op,x}\ .\ S_x\ .N\right)\right] \quad \text{Equation 5}$$

Configuration 3 shares similar constraints that applied to Configuration 1. The difference lies in the electricity supply, which in this case is from the electricity grid. The Energy balance constraint is expressed in Equation (6). It equates the sum of the electricity purchase from the grid, $E_{Grid,buy}(t)$ and battery discharge at any time step to the sum of the energy consumption by the electrolyser, compressor and battery charging.

$$\forall t : E_{Grid,buy}(t) + \eta_{dis}\ .\ B_{dis}(t) = E_{EL}(t) + E_{comp}(t) + \frac{B_{ch}(t)}{\eta_{ch}} \quad \text{Equation 6}$$

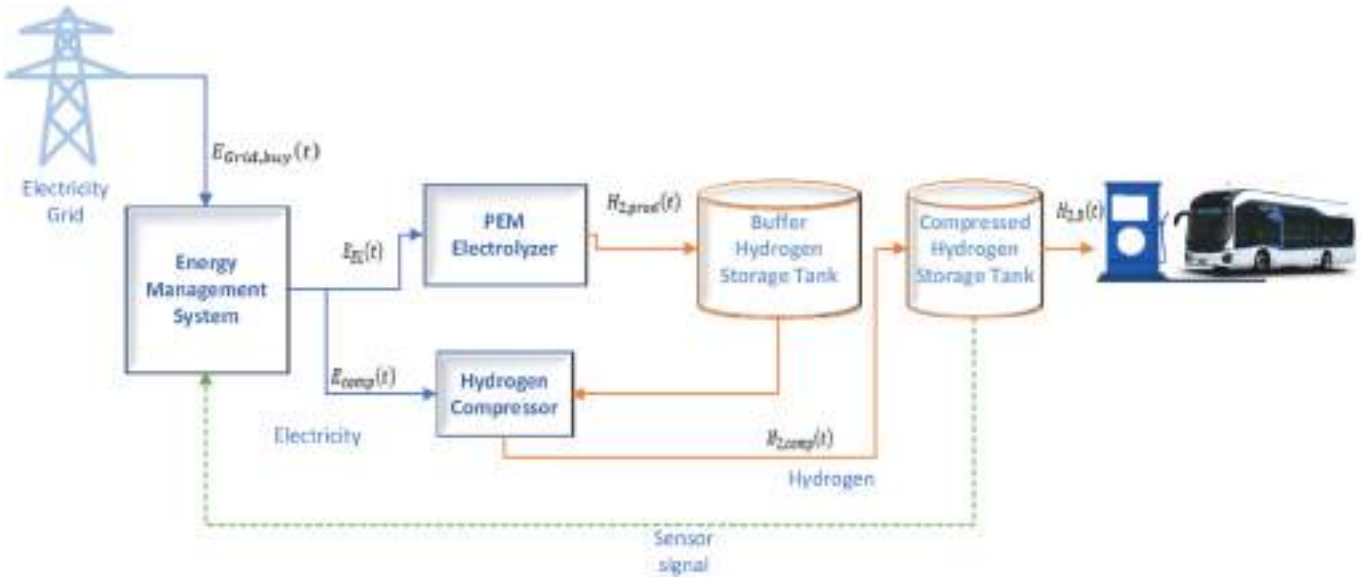

Fig. 5. Schematic diagram of Configuration 3.

4.3. Bi-directional grid interactive renewable energy system

Configurations 4 and 5 illustrated below consist of a grid-connected, hybrid renewable energy system, where excess renewable energy production is sold to the grid through the wholesale electricity market as shown in Fig. 6. Moreover, the bi-directional grid interactivity has the potential to support optimal grid operation by flattening the duck curve, offering balancing services or local flexibility support, depending on scale.

4.3.1. Problem formulation - configuration 4

In the case of Configuration 4, the electricity cost structure comprises of annualized investment cost and wholesale electricity prices. The objective of the optimization problem is expressed in Equation (7). The total cost is expressed as the sum of the grid electricity purchase (including grid charges and carbon price) and the capital and fixed operating costs of each component. The revenue from electricity sales to the grid, $E_{Grid,sale}(t)$ over all time step t is subtracted.

$$\textit{minimize } TC = N \cdot \sum_{t=1}^{T} \left(E_{Grid,buy}(t) \cdot \left(p_{Grid}(t) + F_{Grid} + I_{CO2} \cdot C_{CO2}\right)\right) - N \cdot \sum_{t=1}^{T} \left(E_{Grid,sale}(t) \cdot \left(p_{Grid}(t) - F_{Grid}\right)\right) + \sum_{x \in X} \left[\left(R_x \cdot C_{cap,x} \cdot S_x\right) + \left(C_{op,x} \cdot S_x \cdot N\right)\right] \quad \text{Equation 7}$$

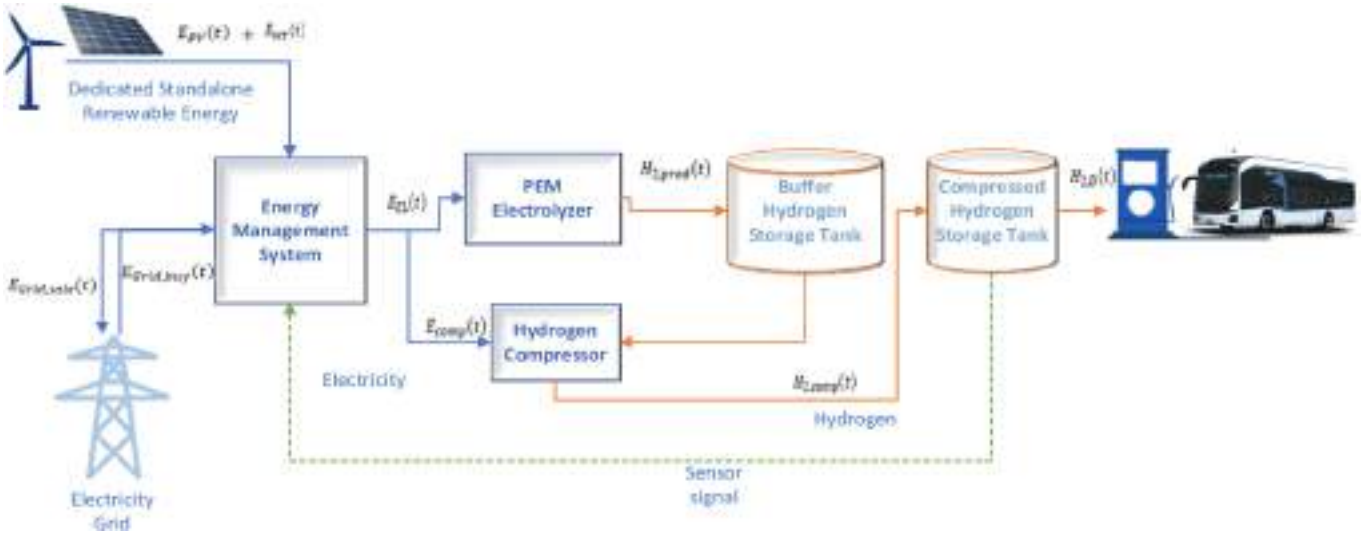

Fig. 6. Schematic diagram of Configurations 4 and 5.

Equation (8) is the energy balance constraint which, unlike the previous configurations discussed, include the energy sold to the grid. This constraint ensures that the energy-consuming components do not use more energy than it has available and that any excess energy is either used for battery charging or sold to the grid.

$$\forall t : E_{Grid,buy}(t) + E_{PV}(t) + E_{WT}(t) + \eta_{dis} \,.\, B_{dis}(t) \geq E_{EL}(t) + E_{comp}(t) + \frac{B_{ch}(t)}{\eta_{ch}} + E_{Grid,sale}(t) \quad \text{Equation 8}$$

The objective function minimizes total costs which comprises the sum of electricity purchase costs through the PPA agreements and the costs of installing and maintaining the electrolyser and storage infrastructure, and subtracting the revenue from electricity sales to the grid across the period. The objective function is expressed in Equation (11) below:

$$\begin{aligned} minimize\ TC = N \,.\, \sum_{t=1}^{T} \left(E_{WT}(t) \,.\, PPA_{wind} + E_{PV}(t) \,.\, PPA_{solar} \right) \\ + \sum_{x\ \epsilon\ X} \left[\left(R_x \,.\, C_{cap,x} \,.\, S_x \right) + \left(C_{op,x} \,.\, S_x \,.N \right) \right] \\ + N \,.\, \sum_{t=1}^{T} \left(E_{Grid,buy}(t) \,.\, (p_{Grid}(t) + F_{Grid} + I_{CO2} \,.\, C_{CO2}) \right) - N \,.\, \sum_{t=1}^{T} \left(E_{Grid,sale}(t) \,.\, (p_{Grid}(t) - F_{Grid}) \right) \end{aligned} \quad \text{Equation 11}$$

In addition, *the* electricity purchased from the grid has to be lower than the sum of the consumption from the electrolyser, compressor, and battery charge as expressed in Equation (9). This constrain prevents unnecessary grid consumption and maintains a balanced energy system.

$$\forall t : E_{Grid,buy}(t) \leq E_{EL}(t) + E_{comp}(t) + \frac{B_{ch}(t)}{\eta_{ch}} \quad \text{Equation 9}$$

Lastly, Equation (10) describes a constraint on the electricity sold to the grid. It can be any amount from zero up to the maximum power, P_{max}, only if two conditions are met:

1. The forecasted load on the grid at time *t*, $L_{Grid}\ (t)$, is greater than the minimum benchmark load for grid injection across all time steps, $L_{Grid,bench}$. This ensures that electricity is sold to the grid when the grid demand is higher than usual, indicating a need for more power. The median annual grid load serves as $L_{Grid,bench}$ in this model.
2. The day-ahead price at time *t*, $p_{Grid}(t)$, is greater than the minimum benchmark day-ahead price across all time steps, $p_{Grid,bench}$. High electricity price serves as an indicator of high demand and a need for the injection of power production into the grid. This has the additional advantage of maximizing the revenue from electricity sales. The median annual day-ahead price serves as $p_{Grid,bench}$ in this model.

This constraint provides a mechanism for managing electricity sales to the grid, ensuring that sales take place primarily during periods of high demand. This strategy exemplifies how the hydrogen hub can bolster grid stability, contributing renewable electricity precisely when it is most crucial—during peak load hours.

$$\forall t : \begin{cases} 0 \leq E_{Grid,sale}(t) \leq P_{max} & if\ p_{Grid}(t) > p_{Grid,bench}\ and\ L_{Grid}\ (t) > L_{Grid,bench} \\ E_{Grid,sale}(t) = 0 & otherwise \end{cases} \quad \text{Equation 10}$$

4.3.2. Problem formulation - configuration 5

Configuration 5 employs an "as-produced" financial PPA, where the green hydrogen hub enters a long-term contract with a renewable energy generator. The difference with Configuration 2 is that the green hydrogen hub can trade excess renewable generation to the grid. Similar to the structure of Configuration 2, this agreement reduces capital cost and provides a predictable cost and revenue framework for the green hydrogen hub, acting as a buffer against energy price volatility inherent in Configuration 3. Consequently, Configuration 5 offers a balance between the flexibility and grid support advantages of Configuration 4, and the financial stability, reduced capital expenditure, and risk management benefits offered by a PPA structure.

All the constraints applied to Configuration 4 similarly apply to Configuration 5.

4.4. Summary of the configurations

The optimal solutions obtained for each configuration are finally compared with each other from an economic point of view using the Levelized Cost of Hydrogen (LCOH). This is a widely used technique for determining the actual cost of producing Hydrogen. To compute the LCOH, the annualized total cost is divided by the annual hydrogen production from the green hydrogen hub, adopting the method in Ref. [87]. Table 4 provides a summary of the five green hydrogen hub configurations considered.

5. Results and Discussions

This section presents the results of five green hydrogen hub configurations considered in this study. Firstly, Section 5.1 describes the optimal design of the green hydrogen hub in the French case study while Section 5.2 shows some details on operation for each configuration. Following on from this point, Section 5.3 assesses the economic viability of each configuration for transport decarbonization. Finally, Section 5.4 analyses the LCOH and optimal design sensitivity to changes in energy prices and to the location of the green hydrogen hub in five European cities (see Tables 2 and 3).

5.1. Optimal system capacity sizing and operation

The capacity for all components results from optimal capacity sizing of the optimization model except for the PV and wind capacity in Configurations 2 and 5 (involving PPAs), which are based on heuristics. This is to reflect realistic capacity sizing associated with the nature of the electricity cost structure. Across both configurations that are optimally sized, a hybrid renewable energy system is optimal. This is due to the complementary nature of wind and solar resources in the location considered. All configurations are observed to have the same optimal electrolyser, compressor, and buffer storage capacity. Configuration 4 which offers grid interaction and optimal PV and wind capacity requires the lowest compressed storage capacity while Configuration 1 has the highest storage capacity requirement since it cannot rely on grid electricity when wind and solar resources are unavailable and it avoids oversizing PV and wind capacity unlike Configurations 2 and 4. Configuration 4 has higher optimal PV and wind capacities than Configuration 1 due to the high wholesale electricity price, which promotes electricity sales to the grid, making slight oversizing optimal.

Table 4
Summarizes the key features of each configuration.

Parameter	Config 1	Config 2	Config 3	Config 4	Config 5
Electricity Source	PV, Wind	PV, Wind	Grid	PV, Wind, Grid	PV, Wind, Grid
Electricity Cost Structure	Capex (Installation Costs)	Opex (PPA)	Opex (Wholesale electricity market)	Capex (Installation Costs), Opex (Wholesale electricity market)	Opex (PPA, Wholesale electricity market)
Bi-directional Power Flow	No	No	No	Yes	Yes
Renewable Energy Capacity Sizing	Optimal	Based on Heuristics	Not Applicable	Optimal	Based on Heuristics
Other components	Electrolyser, Compressor, Buffer Storage, Compressed Storage, Refrigerator, Dispenser	Same as Config 1	Same as Config 1	Same as Config 1	Same as Config 1

Table 5
Summary of optimal capacity for Configurations 1–5 for baseline case study.

System Component	Config 1	Config 2	Config 3	Config 4	Config 5
PV Capacity (MW)	11.12	15.00	–	11.77	15.00
Wind Capacity (MW)	12.77	15.00	–	15.14	15.00
Electrolyser Capacity (MW)	10.44	10.44	10.44	10.44	10.44
Buffer Storage Capacity (kg)	100	100	100	100	100
Compressed Storage Capacity (kg)	5973	3953	4245	3323	3953
Compressor capacity (kg/h)	170	170	170	170	170
Battery Capacity (kWh)	0	0	0	0	0

None of the configurations include a battery energy storage system for optimal sizing due to the high cost per MW, instead preferring compressed hydrogen storage. Across all configurations, the electrolyser capacity factor is about 38%, which is in line with the findings in academic literature [88]. Electrolyser is the main consumer of electricity and compressor consumption represents only about 4% of total electricity consumption. Due to this negligible contribution, the compressor does not contribute significantly to the energy demand or flexibility of the system. Table 5 presents the component capacity sizing for the five configurations of green hydrogen hubs. To illustrate the operation of the different green hydrogen hub configurations, a typical winter week (first week of January) and a typical summer week (first week of July) are utilized.

5.1.1. *Configurations 1 and 2*

Fig. 7 depicts the hourly energy production and consumption, as well as the compressed hydrogen storage level, for Configuration 1. Since the only difference between Configurations 1 and 2 is in the cost structure, the operation of both configurations is similar. Energy production and consumption are represented by positive and negative axes, respectively. As expected, the winter week highlights high wind energy production but low PV output while the summer week has high and consistent PV production during the day, and wind energy output is less consistent. As illustrated in Fig. 7, the electrolyser's power consumption increases during periods of high renewable energy production and decreases when production is low. Moreover, the electrolyser and compressor power consumption is more intermittent during the winter week than in the summer week, which can be attributed to the volatile nature of the predominant wind energy during the winter week. As configuration 1 is designed to optimize the PV and wind capacities to meet hydrogen demand, there are no periods when the electrolyser consumption exceeds the available energy production.

The renewable electricity curtailment is about 40% for Configuration 1 and 51% for Configuration 2 (due to non-optimal renewable capacity sizing), indicating significant excess power production. This is

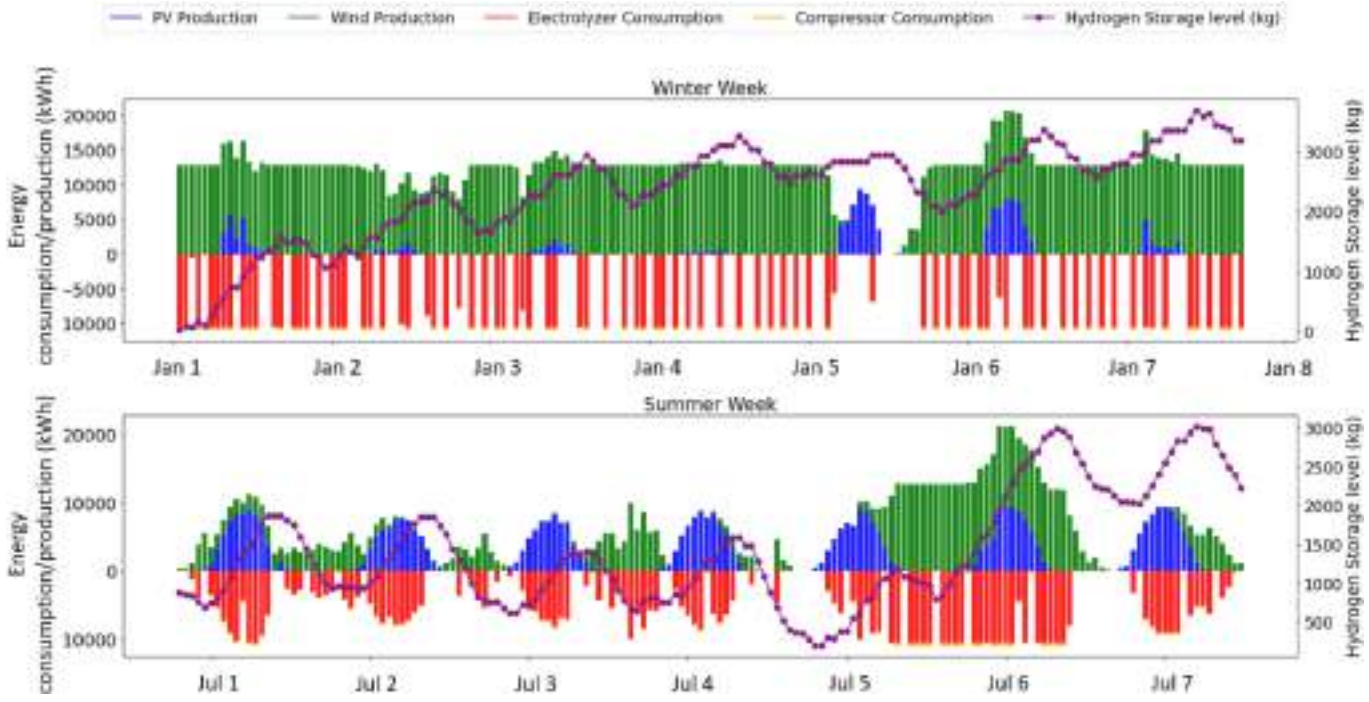

Fig. 7. Operating pattern of Configuration 1 in typical winter and summer week.

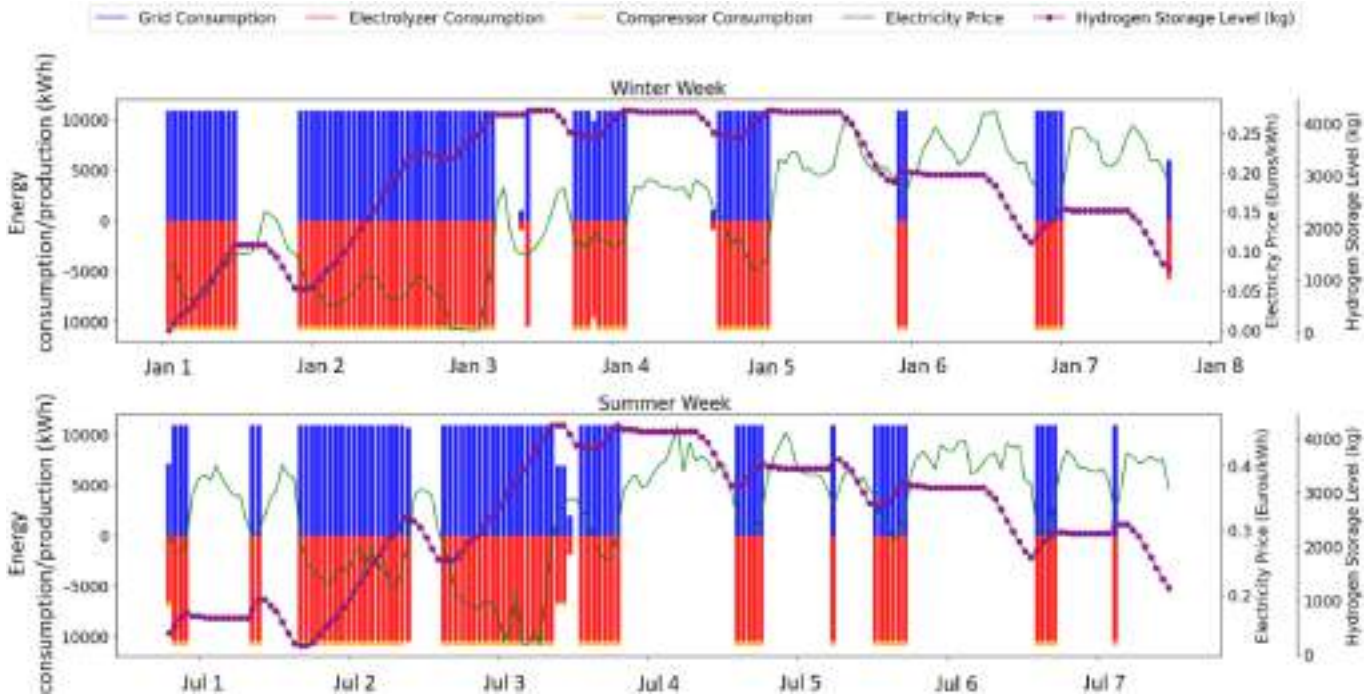

Fig. 8. Operating pattern of Configuration 3 in typical winter and summer week.

particularly obvious during the winter due to high wind production and limited flexibility of the configuration. The hydrogen storage tank serves as the only source of flexibility. The hydrogen storage level illustrated by the purple line shows cyclical increases and decreases, indicating that despite the complementary nature of wind and PV, there remains a temporal mismatch between hydrogen production and demand, necessitating compressed hydrogen storage to balance this mismatch. The steady increase in hydrogen storage level observed in the winter week is due to the initial empty state of the compressed storage tank.

5.1.2. *Configuration 3*

Fig. 8 illustrates power production and consumption patterns in Configuration 3 as well as the hydrogen storage level over the winter and summer weeks. The results highlight that despite the grid's ability to provide power on-demand, Configuration 3, like the other configurations studied, still relies on compressed hydrogen storage for cost-effective operation. Hydrogen storage enables the green hydrogen hub to decouple hydrogen production from demand, avoiding expensive hydrogen production during periods of high electricity prices and allowing a higher capacity factor for the electrolyser. This behaviour is further demonstrated by the negative correlation between hydrogen storage levels (purple dotted line) and electricity prices (green line). The power consumption of the electrolyser peaks during the late night to early morning period (22–5) and exhibits some activity during midday (12–16). In contrast, there is little to no consumption during the evening hours (17–20) and minimal consumption in the morning (7–10). Notably, these periods of low consumption coincide with periods of high grid electricity demand and high electricity prices. By primarily operating during off-peak periods, when electricity is cheaper (often due to low electricity demand and high production from renewable sources like wind and solar), the operational strategy of the electrolyser aligns with the optimal utilization of the electricity grid.

5.1.3. *Configurations 4 and 5*

Fig. 9a shows the hourly fluctuations in power production, power consumption, electricity prices and the hydrogen storage level over a typical winter and summer week for Configuration 4, but is also representative of Configuration 5 since they differ primarily in their cost structure. The power production sources include PV, wind, and the electricity grid while the power consumption accounts for electrolyser consumption, compressor consumption, and electricity sale to the grid. During the winter week considered, there appears to be no grid consumption or sale. On the other hand, the summer week shows some periods of electricity sales to the grid. Grid consumption does not take place during the selected weeks but occurs at other periods in the year. The hydrogen storage level varies inversely with electricity price, indicating that hydrogen is produced and stored when electricity is cheaper and used when electricity is more expensive.

Fig. 9b shows the relationship between power consumption, grid interaction by the system, the day-ahead electricity prices and expected grid load on an average 24-h period. The negative normalized power indicates power consumption from the grid while the positive axis represents surplus electricity sales to the grid. It can be observed that electricity sale occurs during periods of relatively high electricity prices and/or grid load, particularly during the evening peak load (18–20). In contrast, electricity consumption from the grid occurs predominantly during the late night and early morning periods (0–5). This operational strategy capitalizes on price arbitrage opportunities, enhancing the system's economic viability while benefiting grid stability. Renewable electricity curtailment is 37% and 41% for Configurations 4 and 5, respectively. The remaining underutilization of renewable energy production is attributed to the model's constraints, which restrict electricity sales to the grid when the electricity price is low (an indicator of excess electricity supply) to realistically estimate the revenue potential of the green hydrogen hub. Fig. 9c illustrates the role of hydrogen storage tanks in managing the temporal mismatch between hydrogen production and demand.

5.2. *Economic performance*

The LCOH across all configurations ranged from 4 to over 20 €/kg H_2, indicating the significant impact of the electricity supply configuration on hydrogen cost. Fig. 10 illustrates the contribution of individual components to the LCOH for each configuration. Most notably, Configuration 3 exhibits the highest LCOH, exceeding 20 €/kg H_2 when the 2022 electricity price is used. The steep cost can be attributed to the

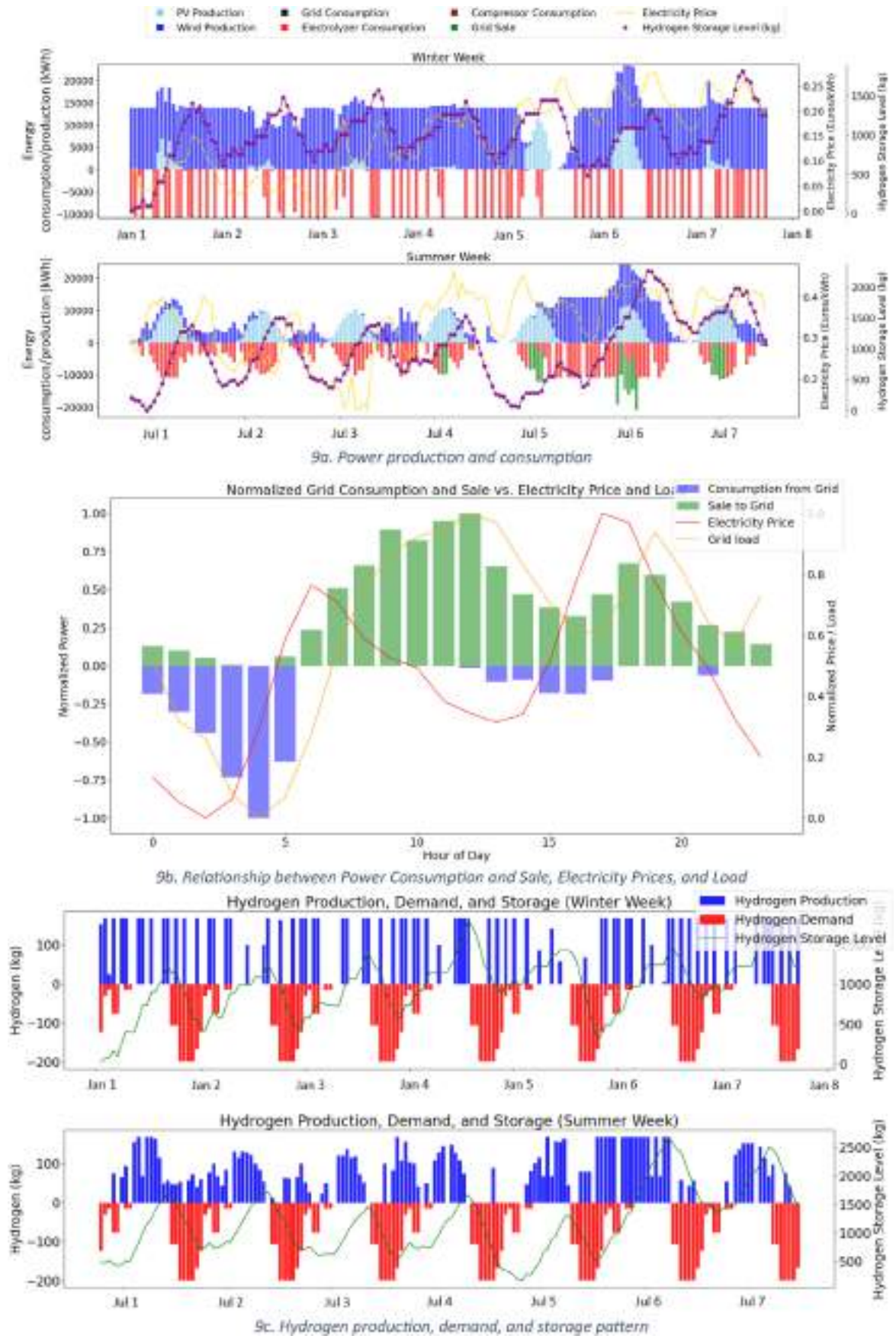

Fig. 9. Operating pattern of Configuration 4 during the typical winter and summer week.

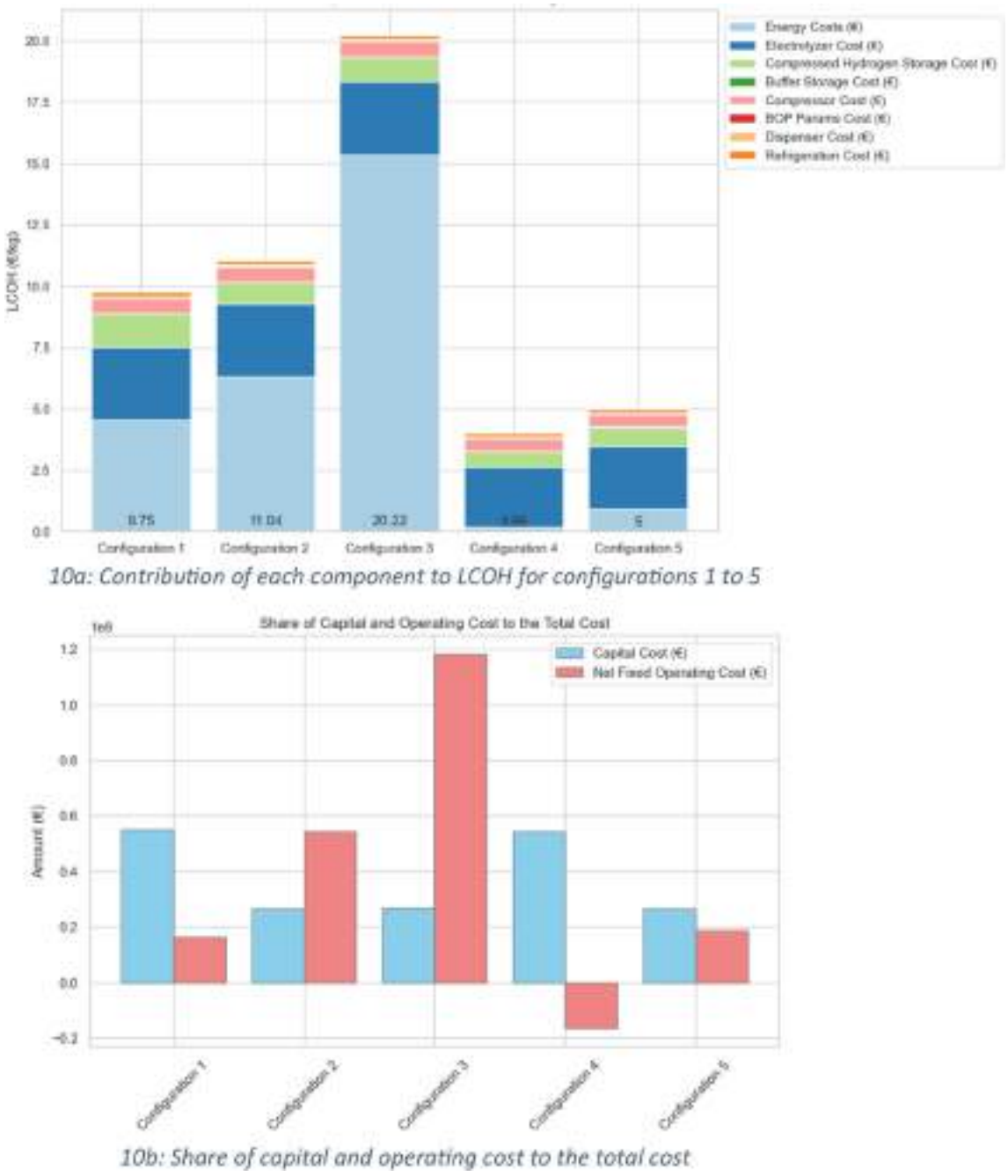

Fig. 10. Cost structure of Configurations 1 to 5.

2022 energy crisis in Europe as the LCOH for the same Configuration 3 is 11.64 and 10.70 €/kg H_2 when analyzed for the years 2021 and 2023 respectively. In configuration 3, energy costs represent over 75% of the LCOH, as depicted in Fig. 10a. In contrast, Configurations 4 and 5 have the lowest LCOH, primarily due to the revenue derived from selling surplus electricity to the grid. Specifically, Configuration 4 benefits from optimally sized PV and wind capacities, reducing the net energy cost contribution to the LCOH to less than 5%. Similarly, Configurations 2 and 5 are economically favourable due to lower capital costs due to Power Purchase Agreement (PPA) structure as shown in Fig. 10b, where their capital cost is less than half of that of Configurations 1 and 4. In Configurations 1, 2, and 3, energy costs account for the largest portion of the LCOH, while in Configurations 4 and 5, the electrolyser represents the most significant cost. In Configurations 1 and 2, PV and wind constitute the entire energy costs, with wind costs taking the larger share of both. The costs of PV and wind in Configuration 1 are less than those in Configuration 2, due to optimal capacity sizing in the former.

5.3. Sensitivity of LCOH

This section observes the sensitivity of the LCOH and optimal capacity mix to a range of factors such as the geographical location, the investment cost of critical components, the prevailing wholesale electricity market price, and the temporal distribution of hydrogen demand. We focus on parameters that are influenced by energy supply configuration.

5.3.1. Sensitivity of LCOH to location and hydrogen demand profile

Fig. 11 illustrates the variation of the LCOH of Configurations 1–5 to both location and hydrogen demand profile. In both hydrogen demand

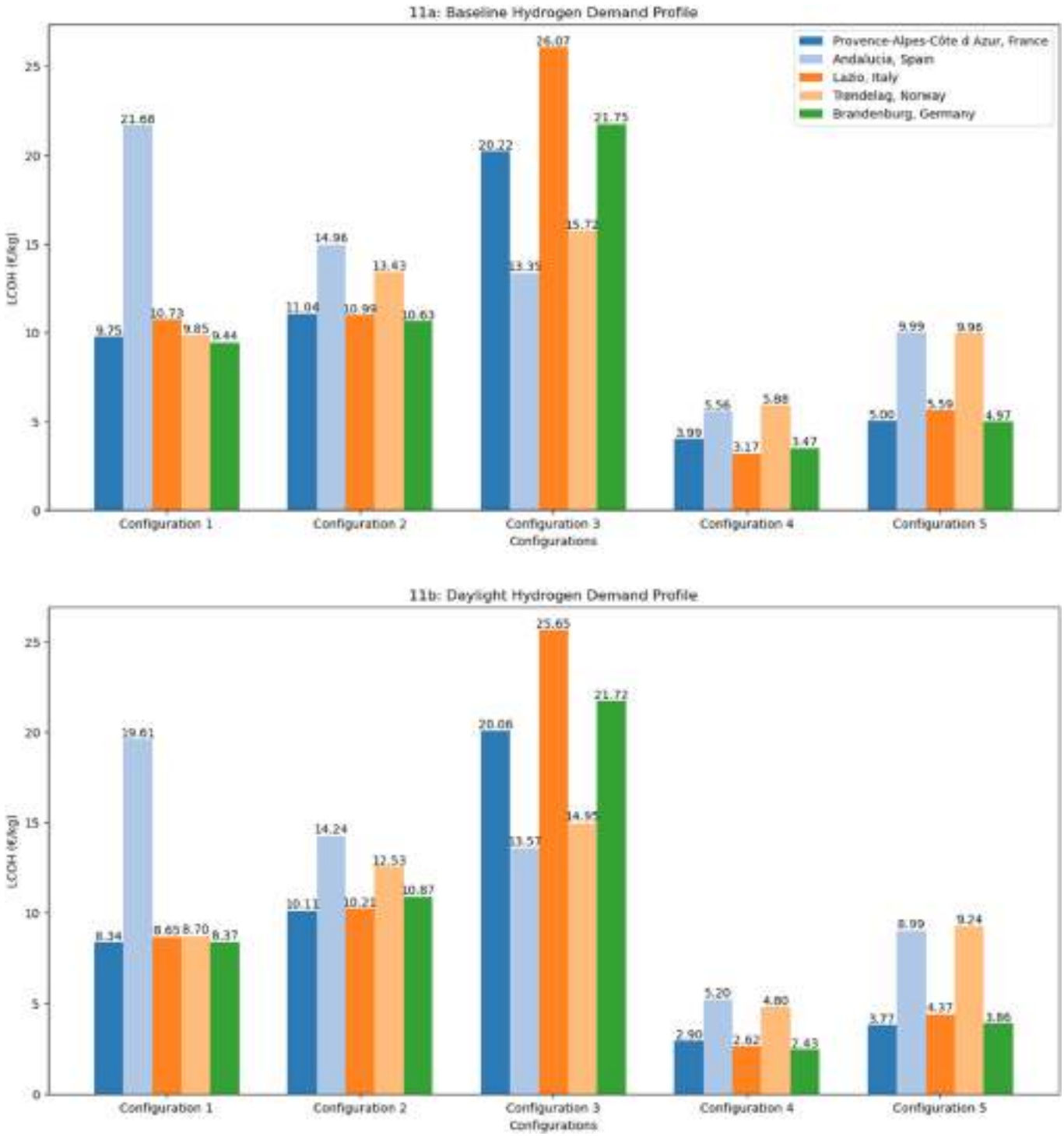

Fig. 11. Sensitivity of LCOH to location and hydrogen demand profile for Configurations 1-5.

profiles, the LCOH varies significantly across configurations and locations. Configuration 3 has the highest LCOH across most locations due to high electricity costs while configuration 4 delivers the lowest LCOH. The low LCOH of configuration 4 is due to the sale of surplus electricity to the grid during peak periods. Andalucia and Trondelag have relatively high LCOH in most configurations, indicating that they may not be suitable for green hydrogen-based urban transport decarbonization. Conversely, Brandenburg, Côte d'Azur and Lazio demonstrate potential benefits from fuel-cell urban bus fleet deployment.

When considering the deployment of green hydrogen infrastructure for urban transport decarbonization, Configurations 4 and 5 are shown to be the most cost-optimal with Côte d'Azur having an LCOH of 5 €/kg in baseline hydrogen demand profile of configuration 5, and further reducing to 3.77 €/kg under the daylight hydrogen demand profile. The baseline hydrogen demand profile represents the current predominant hydrogen demand profile for fuel-cell electric bus fleets in Europe [56]. However, it can be observed in Fig. 11b that considerable cost reductions in LCOH across almost all locations and configurations can be derived by adjusting the hydrogen demand profile to daylight hours to better align with solar energy availability, leading to a decrease in hydrogen storage capacity requirements. It may be worth considering a better synergy between the temporal distribution of hydrogen demand

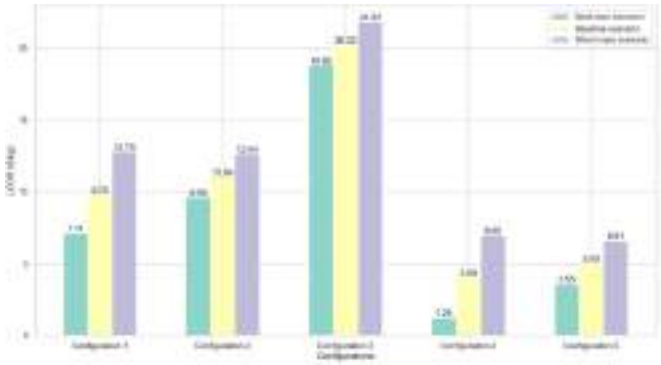

12a. Sensitivity to different investment cost scenarios

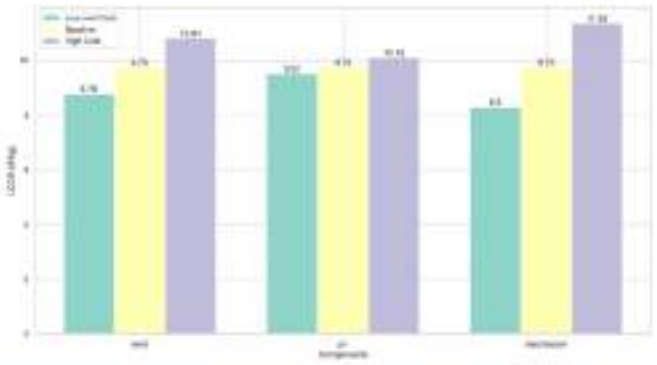

12b Sensitivity of Configuration 1 to component cost scenarios

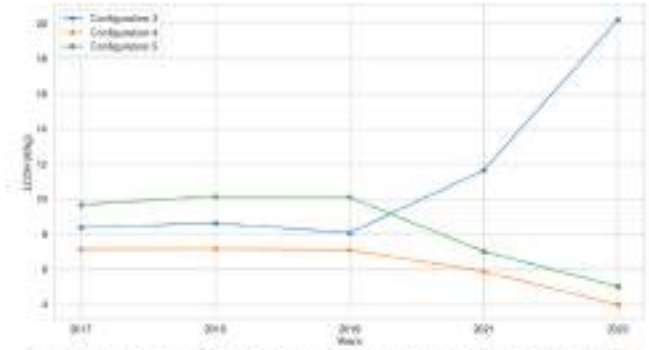

12c. Sensitivity of LCOH to wholesale electricity prices using day-ahead market price between 2017-2022

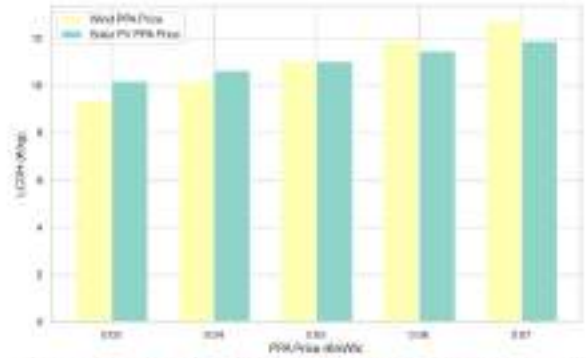

12d. Sensitivity of LCOH to PPA price for Configuration 2

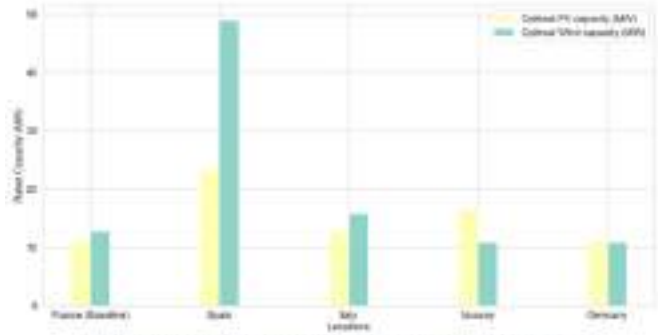

12e.Sensitivity of optimal PV and wind capacity to geographical location for Configuration 1

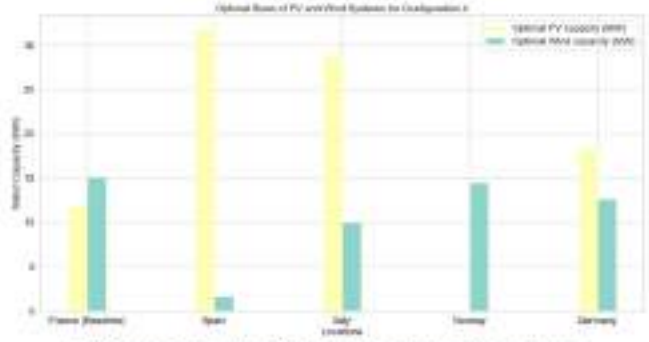

12f. Sensitivity of optimal PV and wind capacity to geographical location for Configuration 4

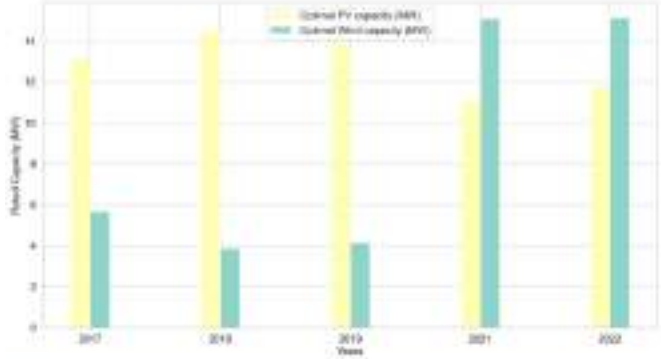

12g. Sensitivity of optimal PV and wind capacity to electricity prices for Configuration 4.

Fig. 12. Sensitivity to infrastructure and electricity cost assumptions.

by the bus fleet and the geographical location to minimize the hydrogen production-demand mismatch, and thus, further reduce the LCOH.

5.3.2. Sensitivity of LCOH and optimal capacity mix to investment cost scenarios and electricity price

As observed in Fig. 10, electricity and electrolyser costs make up the largest share of the green hydrogen production costs. Fig. 12a presents a sensitivity analysis for each configuration, considering various cost scenarios. These scenarios include optimistic, baseline, and worst-case cost assumptions for wind, PV, and electrolyser components as defined in Refs. [66,67]. Notably, Configurations 1 and 4 exhibit the highest sensitivity to investment cost variations. This is attributable to the electricity cost structure in these configurations, involving annualized investment costs for renewable energy infrastructure. Under the best-case scenario, Configuration 4 delivers an LCOH as low as 1.24 €/kg H_2. However, under the worst-case scenario, the LCOH increases to more than five times this amount, showing a significant range of LCOH depending on cost assumptions.

The sensitivity of Configuration 1 to PV, wind and electrolyser cost assumptions are further investigated separately and illustrated in Fig. 12b. The results indicate that electrolyser costs yield the highest sensitivity ahead of PV and wind. This is generalizable across all configurations considered since Configuration 1 has the highest capital expenditure for PV and wind. This can be attributed to the nascent state of electrolyser technology; significant cost reductions, reflected in the best-case scenario, are anticipated as the technology advances and economies of scale are realized in hydrogen production via electrolysis.

Additionally, as shown in Fig. 12c, the LCOH for Configuration 3 more than doubled from 8€/kg H_2 in 2019 to 20.2€/kg H_2 in 2022 and significantly decreased to 10.7 €/kg H_2 in 2023. This illustrates the sensitivity of configuration 3 to wholesale electricity prices. By contrast, Configurations 3 and 4 benefit from increased electricity prices since these configurations sell electricity back to the grid at higher prices, thus increasing revenue from electricity sales, and further reducing net energy costs. Fig. 12d illustrates the sensitivity of the LCOH of Configuration 2 to the PPA price of wind and PV, with the LCOH showing greater sensitivity to wind PPA price.

Furthermore, the optimal sizing of renewable energy assets for the green hydrogen hub configurations considered varies depending on factors such as location and electricity price. Fig. 12d and e show the optimal renewable capacity mix across various locations. The optimal renewable capacity mix differs greatly depending on location. For each location, the optimal renewable capacity mix also differs significantly. Norway stands out with significant PV capacity in configuration 1 and none in configuration 4.

Additionally, the optimal renewable capacity mix is sensitive to electricity prices as observed in Fig. 12g. High wholesale electricity prices, as experienced since 2021, favour the oversizing of renewable energy assets to facilitate revenue generation through electricity sales to the grid. Conversely, during periods of low grid prices, such as those observed from 2017 to 2019, it is optimal to undersize renewable energy assets, and instead purchase electricity from the grid. The high sensitivity to electricity costs makes it crucial to consider the uncertainties in future electricity prices when considering the design of green hydrogen hubs.

6. Conclusion

The techno-economic analysis carried out in this study presents an approach to analyzing and comparing different energy supply configurations for an on-site hydrogen refuelling station designed for decarbonizing a fleet of fuel-cell buses. Through the extraction of relevant data, linear programming-based problem formulation and implementation in Python-based Pyomo, and subsequent cost and results analysis, the developed computational tool facilitates location-specific techno-economic assessments for green hydrogen hubs with a focus on energy supply management. The comparative techno-economic evaluation of five different energy supply configurations for green hydrogen hubs, commonly used in academic literature, led to a better understanding of their technical and economic performance. In the baseline case study, the LCOH ranged from 4 to 20 €/kg H_2 illustrating the importance of careful consideration of electricity supply configuration. Sensitivity analysis is carried out to understand the impact of varying conditions, ranging from investment cost scenarios, wholesale electricity market prices, the hydrogen demand patterns, to geographic location.

The findings highlight that Configurations 4 and 5 (grid-interactive systems) consistently achieve the lowest LCOH across all geographical locations considered, due to the additional flexibility offered by bi-directional grid interaction. This enables them to optimally size renewable capacities and generate additional revenue from electricity sales to the grid. However, the sensitivity analysis underlines the susceptibility of grid-reliant configurations to unpredictable electricity market prices. Configurations that utilize annualized investment costs incur significant capital costs, but very low operating costs. As such, they are highly susceptible to changes in component costs. On the other hand, configurations that utilize PPA for renewable electricity offer a balance between capital and operating costs, even though, their total cost may be higher. Configuration 5 (grid-interactive PPA) particularly offers a unique opportunity to benefit from both the flexibility of grid connection and low capital cost due to PPAs.

Since the study considered only five configurations, opportunities abound to further explore the decarbonization of urban bus fleets. Future work could build upon this foundation by incorporating stochasticity in certain parameters and expanding the configurations to include the sharing of renewable energy infrastructure with a renewable energy community or electric bus fleet charging station, potentially reducing curtailed renewable electricity. Further work can also explicitly co-optimize green hydrogen hub planning and operations with route planning of urban bus fleets to derive an optimized hydrogen demand schedule.

In summary, the detailed modelling and analysis conducted in this study provide valuable insights into different electricity supply strategies to power green hydrogen hubs, focusing on their potential to decarbonize public transport bus fleets in Europe. The results emphasize the need for customized planning and taking advantage of sector coupling and alternative cost structures in deploying and operating green hydrogen hubs. As European cities actively seek to reduce transportation sector carbon emissions, the insights from this study can inform private investors and policymakers on green hydrogen infrastructure deployment for metropolitan bus fleet decarbonization.

CRediT authorship contribution statement

Kamaldeen Adekola: Writing – review & editing, Writing – original draft, Visualization, Software, Project administration, Methodology, Investigation, Formal analysis, Data curation, Conceptualization. **Samim Ghafoori:** Writing – review & editing, Validation, Project administration, Methodology, Funding acquisition, Conceptualization. **François Dechamp:** Writing – review & editing, Validation, Resources. **Alessandro Prada:** Writing – review & editing, Validation, Methodology.

Declaration of competing interest

The authors declare that they have no known competing financial interests or personal relationships that could have appeared to influence the work reported in this paper.

Acknowledgement

This research received financial support from ABMI Engineering Company.

Appendix

A. Common Constraints

The following constraints and relationships are used across all configurations.

$$E_{PV}(t) = e_{PV}(t) \cdot PV_{size} \quad \text{A.1}$$

$$E_{WT}(t) = e_{WT}(t) \cdot WT_{size} \quad \text{A.2}$$

$$E_{EL}(t) = H_{2,prod}(t) \cdot e_{EL,H2} \cdot \eta_{EL} \quad \text{A.3}$$

$$E_{comp}(t) = H_{2,comp}(t) \cdot e_{comp,H2} \quad \text{A.4}$$

A.4, $e_{comp,H2}$ is the power required to compress a unit kg of hydrogen from the exit of the PEM electrolyser at 30 bar–500 bar required for fuel dispensing and high pressure storage.

Electrolyser maximum capacity constraint in A.5 limits the electricity input of the electrolyser to its rated capacity, EL_{size}.

$$\forall t : E_{EL}(t) \leq EL_{size} \quad \text{A.5}$$

The *global hydrogen balance* in A.6 ensures that the sum of hydrogen production, $H_{2,prod}(t)$ in a year is at least equal to the sum of hydrogen demand $H_{2,D\ (t)}$ in the same year.

$$\forall t : \sum_{t} H_{2,prod}(t) \geq \sum_{t} H_{2,D}(t) \quad \text{A.6}$$

A.7 requires the compressed hydrogen storage level, $SL_{H2,comp}$ from the previous time step (*t-1*) to be sufficient to meet the hydrogen demand at the current time step. However, this constraint only applies for time steps greater than 1 (t > 1), allowing the system to initialize hydrogen production.

$$\forall t > 1 : SL_{H2,comp}(t-1) \geq H_{2,D}(t) \quad \text{A.7}$$

A.8 ensures that the changes in the hydrogen storage level $SL_{H2,prod}$ from one time step to the next are accurately accounted for based on the amount of hydrogen produced, $H_{2,prod}(t)$ and the amount compressed, $H_{2,comp}(t)$ at any given time t.

$$\begin{aligned} SL_{H2,prod}(0) &= S_0 + H_{2,prod}(0) - H_{2,comp}(0) \\ \forall t > 0 : SL_{H2,prod}(t) &= SL_{H2,prod}(t-1) + H_{2,prod}(t) - H_{2,comp}(t) \end{aligned} \quad \text{A.8}$$

A.9 caps the maximum level of hydrogen storage at any given time, $SL_{H2,prod}(t)$ to the capacity of the buffer storage, $S_{LP,size}$. Due to the low energy density of hydrogen at 30 bar, the buffer storage's maximum capacity, $S_{LP,max}$ is set at 100 kg in A.10 to ensure a feasible physical volume for the storage. The constraint is mathematically represented as follows:

$$\forall t : SL_{H2,pr\ od}(t) \leq S_{LP,size} \quad \text{A.9}$$

$$S_{LP,size} \leq S_{LP,max} \quad \text{A.10}$$

A.11 accounts for the dynamic operation of the compressed hydrogen storage throughout the time steps. This is done by considering the amount of hydrogen compressed, $H_{2,comp}(t)$ amount utilized, $H_{2,D}(t)$ at any given time *t*.

$$\begin{aligned} SL_{H2,comp}(0) &= S_0 + H_{2,comp}(0) - H_{2,D}(0) \\ \forall t > 0 : SL_{H2,comp}(t) &= SL_{H2,comp}(t-1) + H_{2,comp}(t) - H_{2,D}(t) \end{aligned} \quad \text{A.11}$$

A.12 limits the storage level of the compressed hydrogen storage, $SL_{H2,comp}(t)$ at any given time *t* to the capacity of the compressed hydrogen storage, $S_{HP,size}$. The constraint can be mathematically expressed as follows:

$$\forall t : SL_{H2,comp}(t) \leq S_{HP,size} \quad \text{A.12}$$

This stipulates that the stored compressed hydrogen should not exceed the storage unit's capacity at any given time. A.13, ensures that the amount of hydrogen compressed at any given time *t* does not exceed the product of the compressor's capacity, $comp_{size}$ and its efficiency, η_{comp}. This constraint can be represented as:

$$\forall t : H_{2,comp}(t) \leq comp_{size} \cdot \eta_{comp} \quad \text{A.13}$$

A.14 governs the state of charge, $B_{SOC}(t)$ of the battery energy storage at every time step *t*. This constraint appropriately accounts for the energy flows associated with battery charge, $B_{ch}(t)$, battery discharge, $B_{dis}(t)$, and the self-discharge of the battery energy storage system. Battery degradation is not considered within the model. Note that battery degradation is not considered within this model. The constraint is formulated as follows:

$$\begin{aligned} B_{SOC}(0) &= B_{ch}(0) - B_{dis}(0) \\ \forall t > 0 : B_{SOC}(t) &= (1 - Selfdischarge) \cdot B_{SOC}(t-1) + B_{ch}(t) - B_{dis}(t) \end{aligned} \quad \text{A.14}$$

A.15 restricts the state of charge, $B_{SOC}(t)$ of the battery energy storage at any time *t* to the battery capacity, B_{size}. This is to ensure it never exceeds the maximum battery capacity.

$$\forall t : B_{SOC}(t) \leq B_{size} \quad \text{A.15}$$

A.16 stipulates that the energy available for charging the battery storage must not exceed the excess energy available at any given time *t*, after accounting for the energy consumed by the electrolyser and the compressor. This constraint can be mathematically formulated as follows:

$$\forall t : \frac{B_{ch}(t)}{\eta_{ch}} \leq E_{WT}(t) + E_{PV}(t) - E_{EL}(t) - E_{comp}(t) \quad \text{A.16}$$

A.17 and A.18 limit battery charging and discharging at each time step, t. The charging power, $B_{ch}(t)$, and discharging power, $B_{dis}(t)$, cannot exceed the battery size, B_{size}, multiplied by the maximum charging, $P_{max,ch}$, and discharging power, $P_{max,dis}$, respectively, both expressed as percentages of the battery size. These constraints can be mathematically expressed as:

$$\forall t : B_{ch}(t) \leq B_{size} \,.\, P_{max,ch} \quad \text{A.17}$$

$$\forall t : B_{dis}(t) \leq B_{size} \,.\, P_{max,dis} \quad \text{A.18}$$

B. Nomenclature

$t \epsilon T$	Set of time steps	hours
$x \epsilon X$	Set of system components	–
TC	Total Cost	€
R_x	Number of replacements	–
S_x	System capacity	kW
$C_{cap,x}$	Capital costs	€
$C_{op,x}$	Operational costs	€
N	Number of operational hours	hours
E_{EL}	Electrolyser power input	kW
E_{PV}	PV system power output	kW
E_{WT}	Wind turbine power output	kW
E_{comp}	Hydrogen compressor power input	kW
B_{ch}	Battery charging power input	kW
B_{dis}	Battery discharging power output	kW
η_{ch}	Battery charging efficiency	%
η_{dis}	Battery discharging efficiency	%
B_{SOC}	Battery state of charge	kWh
B_{size}	Battery capacity	kW
PV_{size}	Photovoltaic system capacity	kW
WT_{size}	Wind Farm Capacity	kW
$S_{LP,size}$	Capacity of the low-pressure storage	kg
$S_{LP,\max}$	Maximum capacity of the low-pressure storage	kg
$S_{HP,size}$	High-pressure storage capacity	kg
$comp_{size}$	Compressor capacity	kg/hr
e_{PV}	Power harvested by unit kW of PV system	kW
e_{WT}	Power harvested by unit kW of wind system	kW
$e_{EL,H2}$	Power required to produce 1 kg of hydrogen	kW
$e_{comp,H2}$	Power required to compress 1 kg of hydrogen	kW
$H_{2,prod}$	Hydrogen output, 30 bar	kg
$H_{2,comp}$	Compressed hydrogen, 500 bar	kg
$H_{2,D}$	Hourly hydrogen demand	kg
$SL_{H2,prod}$	Storage level of produced hydrogen	kg
$SL_{H2,comp}$	Storage level of compressed hydrogen	kg
η_{comp}	Compressor efficiency	%
$Self discharge$	Self-discharge rate of the battery	%
$P_{max,ch}$	Maximum charging power as a percentage of B_{size}	%
$P_{max,dis}$	Maximum discharging power as a percentage of B_{size}	%
PPA_{wind}	Fixed price under the power purchase agreement for wind	€/kWh
PPA_{solar}	Fixed price under the power purchase agreement for solar PV	€/kWh
$E_{Grid,buy}$	Grid electricity purchased	kWh
$p_{Grid}(t)$	Grid electricity price	€/kWh
F_{Grid}	Grid fees	€/kWh
I_{CO2}	Average carbon intensity of the grid	kg CO_2/kWh
C_{CO2}	Carbon price	€/kg CO_2
$E_{Grid,sale}$	Electricity sold to the grid	kWh
L_{Grid}	Forecasted load on the grid	kWh
$L_{Grid,bench}$	Minimum benchmark load for grid injection	kWh
$p_{Grid,bench}$	Minimum benchmark day-ahead price	€/kWh
P_{max}	Grid terminal capacity	kW

References

[1] Nicole M, Marion P. Annual European Union greenhouse gas inventory 1990–2020 and inventory report 2022. Copenhagen: '; May 2022.

[2] Krause J, et al. EU road vehicle energy consumption and CO2 emissions by 2050 – expert-based scenarios. Energy Pol 2020;138(Mar). https://doi.org/10.1016/j.enpol.2019.111224.

[3] Ec A. European strategy for low-emission mobility. Communication from the commission to the European parliament, the council. the European Economic and Social Committee and the Committee of the Regions'; 2016.

[4] European Commission. Proposal for the regulation of the EUROPEAN parliament and of the council. 2023. France.

[5] Gunawan TA, Monaghan RFD. Techno-econo-environmental comparisons of zero- and low-emission heavy-duty trucks. Appl Energy Feb. 2022;308:118327. https://doi.org/10.1016/J.APENERGY.2021.118327.

[6] Peng Z, Wang Z, Wang S, Chen A, Zhuge C. Fuel and infrastructure options for electrifying public transit: a data-driven micro-simulation approach. Appl Energy Sep. 2024;369:123577. https://doi.org/10.1016/J.APENERGY.2024.123577.

[7] Borghetti F, Carra M, Besson C, Matarrese E, Maja R, Barabino B. Evaluating alternative fuels for a bus fleet: an Italian case. Transport Pol Aug. 2024;154:1–15. https://doi.org/10.1016/J.TRANPOL.2024.05.025.

[8] Kim H, Hartmann N, Zeller M, Luise R, Soylu T. Comparative TCO analysis of battery electric and hydrogen fuel cell buses for public transport system in small to midsize cities. Energies Jul. 2021;14(14):4384. https://doi.org/10.3390/EN14144384. 2021, Vol. 14, Page 4384.

[9] Wijayasekera SC, Hewage K, Razi F, Sadiq R. Fueling tomorrow's commute: current status and prospects of public bus transit fleets powered by sustainable hydrogen. Int J Hydrogen Energy May 2024;66:170–84. https://doi.org/10.1016/J.IJHYDENE.2024.04.030.

[10] Axsen J, Pickrell-Barr J. What drives fleets? Organizations' perceived barriers and motivators for alternative-fuel vehicles. Transp Res D Transp Environ Jul. 2024;132:104220. https://doi.org/10.1016/J.TRD.2024.104220.

[11] Genovese M, Fragiacomo P. Hydrogen refueling station: overview of the technological status and research enhancement. J Energy Storage May 2023;61:106758. https://doi.org/10.1016/J.EST.2023.106758.

[12] IEA. The future of hydrogen: report prepared by the IEAfor the G20. Paris, Jun: Japan'; 2019.

[13] Prince-Richard S, Whale M, Djilali N. A techno-economic analysis of decentralized electrolytic hydrogen production for fuel cell vehicles. Int J Hydrogen Energy Sep. 2005;30(11):1159–79. https://doi.org/10.1016/J.IJHYDENE.2005.04.055.

[14] Balat M. Potential importance of hydrogen as a future solution to environmental and transportation problems. 2008. https://doi.org/10.1016/j.ijhydene.2008.05.047.

[15] International Renewable Energy Agency T. Green hydrogen cost reduction scaling up electrolysers to meet the 1.5°C climate goal H 2 O 2 [Online]. Available: www.irena.org/publications, . [Accessed 12 March 2023].

[16] Turner J, et al. Renewable hydrogen production. INTERNATIONAL JOURNAL OF ENERGY RESEARCH Int. J. Energy Res 2008;32:379–407. https://doi.org/10.1002/er.1372.

[17] Nistor S, Dave S, Fan Z, Sooriyabandara M. Technical and economic analysis of hydrogen refuelling. Appl Energy Apr. 2016;167:211–20. https://doi.org/10.1016/j.apenergy.2015.10.094.

[18] Grüger F, Dylewski L, Robinius M, Stolten D. Carsharing with fuel cell vehicles: sizing hydrogen refueling stations based on refueling behavior. Appl Energy Oct. 2018;228:1540–9. https://doi.org/10.1016/J.APENERGY.2018.07.014.

[19] Alavi O, Mostafaeipour A, Qolipour M. Analysis of hydrogen production from wind energy in the southeast of Iran. Int J Hydrogen Energy Sep. 2016;41(34):15158–71. https://doi.org/10.1016/J.IJHYDENE.2016.06.092.

[20] Siyal SH, Mentis D, Howells M. Economic analysis of standalone wind-powered hydrogen refueling stations for road transport at selected sites in Sweden. Int J Hydrogen Energy Aug. 2015;40(32):9855–65. https://doi.org/10.1016/J.IJHYDENE.2015.05.021.

[21] Cardona P, et al. Modelling and operation strategy approaches for on-site hydrogen refuelling stations. Int J Hydrogen Energy Jan. 2024;52:49–64. https://doi.org/10.1016/J.IJHYDENE.2023.08.192.

[22] Minutillo M, Perna A, Forcina A, Di Micco S, Jannelli E. Analyzing the levelized cost of hydrogen in refueling stations with on-site hydrogen production via water electrolysis in the Italian scenario. Int J Hydrogen Energy Apr. 2021;46(26):13667–77. https://doi.org/10.1016/J.IJHYDENE.2020.11.110.

[23] Moran C, et al. A flexible techno-economic analysis tool for regional hydrogen hubs – a case study for Ireland. Int J Hydrogen Energy Aug. 2023;48(74):28649–67. https://doi.org/10.1016/J.IJHYDENE.2023.04.100.

[24] F. Scheepers et al., 'Improving the efficiency of PEM electrolyzers through membrane-specific pressure optimization', doi: 10.3390/en13030612.

[25] Harrison KW, Remick R, Martin GD, Hoskin A. Hydrogen production: fundamentals and case study summaries [Online]. Available: http://www.osti.gov/bridge. [Accessed 16 May 2023].

[26] Taibi E, Miranda R, Vanhoudt W, Winkel T, Lanoix J-C, Barth F. Hydrogen from renewable power: technology outlook for the energy transition [Online]. Available: www.irena.org. [Accessed 13 March 2023].

[27] Slater S, Joos M. H2ME 2, D4.11: assessing the current role of electrolysers in the provision of grid services'. 2021.

[28] Reddi K, Elgowainy A, Rustagi N, Gupta E. Impact of hydrogen refueling configurations and market parameters on the refueling cost of hydrogen. Int J Hydrogen Energy Aug. 2017;42(34):21855–65. https://doi.org/10.1016/J.IJHYDENE.2017.05.122.

[29] Niaz S, Manzoor T, Pandith AH. Hydrogen storage: materials, methods and perspectives. Renew Sustain Energy Rev May 2015;50:457–69. https://doi.org/10.1016/j.rser.2015.05.011.

[30] Mazloomi K, Gomes C. Hydrogen as an energy carrier: prospects and challenges. Renew Sustain Energy Rev 2012;16:3024–33. https://doi.org/10.1016/j.rser.2012.02.028.

[31] Abdalla AM, Hossain S, Nisfindy OB, Azad AT, Dawood M, Azad AK. Hydrogen production, storage, transportation and key challenges with applications: a review. Elsevier Ltd.; Jun. 01, 2018. https://doi.org/10.1016/j.enconman.2018.03.088.

[32] S. Pierre, 'FICHE TECHNIQUE Rendement de la chaîne hydrogène RENDEMENT DE LA CHAINE HYDROGENE'.

[33] Khan TO, Young MA, Mackinnon CB, Layzell CB. The techno-economics of hydrogen compression [Online]. Available: www.transitionaccelerator.ca. [Accessed 22 June 2023].

[34] Minutillo M, Perna A, Forcina A, Di Micco S, Jannelli E. Analyzing the levelized cost of hydrogen in refueling stations with on-site hydrogen production via water electrolysis in the Italian scenario. Int J Hydrogen Energy Apr. 2021;46(26):13667–77. https://doi.org/10.1016/J.IJHYDENE.2020.11.110.

[35] 'J2601/2_201409: fueling protocol for gaseous hydrogen powered heavy duty vehicles - SAE international' [Online]. Available: https://www.sae.org/standards/content/j2601/2_201409/. [Accessed 12 July 2023].

[36] Schnuelle C, Wassermann T, Fuhrlaender D, Zondervan E. Dynamic hydrogen production from PV & wind direct electricity supply – modeling and techno-economic assessment. Int J Hydrogen Energy Nov. 2020;45(55):29938–52. https://doi.org/10.1016/J.IJHYDENE.2020.08.044.

[37] Clarke RE, Giddey S, Ciacchi FT, Badwal SPS, Paul B, Andrews J. Direct coupling of an electrolyser to a solar PV system for generating hydrogen. Int J Hydrogen Energy Mar. 2009;34(6):2531–42. https://doi.org/10.1016/J.IJHYDENE.2009.01.053.

[38] Yates J, et al. Techno-economic analysis of hydrogen electrolysis from off-grid stand-alone photovoltaics incorporating uncertainty analysis. Cell Rep Phys Sci Oct. 2020;1(10):100209. https://doi.org/10.1016/J.XCRP.2020.100209.

[39] Pang Y, Pan L, Zhang J, Chen J, Dong Y, Sun H. Integrated sizing and scheduling of an off-grid integrated energy system for an isolated renewable energy hydrogen refueling station. Appl Energy Oct. 2022;323:119573. https://doi.org/10.1016/J.APENERGY.2022.119573.

[40] Slater S, Joos M. H2ME 2, D4.11: assessing the current role of electrolysers in the provision of grid services'. 2021.

[41] Guinot B, Montignac F, Champel B, Vannucci D. Profitability of an electrolysis based hydrogen production plant providing grid balancing services. Int J Hydrogen Energy Aug. 2015;40(29):8778–87. https://doi.org/10.1016/J.IJHYDENE.2015.05.033.

[42] Caponi R, Bocci E, Del Zotto L. On-site hydrogen refuelling station techno-economic model for a fleet of fuel cell buses. Int J Hydrogen Energy Jun. 2024;71:691–700. https://doi.org/10.1016/J.IJHYDENE.2024.05.216.

[43] Bahou S. Techno-economic assessment of a hydrogen refuelling station powered by an on-grid photovoltaic solar system: a case study in Morocco. Int J Hydrogen Energy Jul. 2023;48(61):23363–72. https://doi.org/10.1016/j.ijhydene.2023.03.220.

[44] Jørgensen C, Ropenus S. Production price of hydrogen from grid connected electrolysis in a power market with high wind penetration. Int J Hydrogen Energy Oct. 2008;33(20):5335–44. https://doi.org/10.1016/J.IJHYDENE.2008.06.037.

[45] Matute G, Yusta JM, Beyza J, Correas LC. Multi-state techno-economic model for optimal dispatch of grid connected hydrogen electrolysis systems operating under dynamic conditions. Int J Hydrogen Energy Jan. 2021;46(2):1449–60. https://doi.org/10.1016/J.IJHYDENE.2020.10.019.

[46] Tang O, Rehme J, Cerin P. Levelized cost of hydrogen for refueling stations with solar PV and wind in Sweden: on-grid or off-grid? Energy Feb. 2022;241:122906. https://doi.org/10.1016/J.ENERGY.2021.122906.

[47] Ceylan C, Devrim Y. Green hydrogen based off-grid and on-grid hybrid energy systems. Int J Hydrogen Energy Feb. 2023. https://doi.org/10.1016/J.IJHYDENE.2023.02.031.

[48] Matute G, Yusta JM, Naval N. Techno-economic model and feasibility assessment of green hydrogen projects based on electrolysis supplied by photovoltaic PPAs. Int J Hydrogen Energy Feb. 2023;48(13):5053–68. https://doi.org/10.1016/J.IJHYDENE.2022.11.035.

[49] Ghiassi-Farrokhfal Y, Ketter W, Collins J. Making green power purchase agreements more predictable and reliable for companies. Decis Support Syst May 2021;144:113514. https://doi.org/10.1016/J.DSS.2021.113514.

[50] Gökçek M, Kale C. Optimal design of a hydrogen refuelling station (HRFS) powered by hybrid power system. Energy Convers Manag Apr. 2018;161:215–24. https://doi.org/10.1016/j.enconman.2018.02.007.

[51] Gökçek M, et al. Optimum sizing of hybrid renewable power systems for on-site hydrogen refuelling stations: case studies from Türkiye and Spain. Int J Hydrogen Energy Mar. 2024;59:715–29. https://doi.org/10.1016/J.IJHYDENE.2024.02.068.

[52] Oyewole OL, Nwulu NI, Okampo EJ. Optimal design of hydrogen-based storage with a hybrid renewable energy system considering economic and environmental uncertainties. Energy Convers Manag Jan. 2024;300:117991. https://doi.org/10.1016/J.ENCONMAN.2023.117991.

[53] Caponi R, Bocci E, Del Zotto L. Techno-economic model for scaling up of hydrogen refueling stations. Energies Oct. 2022;15(20):7518. https://doi.org/10.3390/EN15207518. 2022, Vol. 15, Page 7518.

[54] Coppitters D, Verleysen K, De Paepe W, Contino F. How can renewable hydrogen compete with diesel in public transport? Robust design optimization of a hydrogen refueling station under techno-economic and environmental uncertainty. Appl Energy Apr. 2022;312:118694. https://doi.org/10.1016/J.APENERGY.2022.118694.

[55] Ecosystèmes territoriaux hydrogène : Agnès Pannier-Runacher annonce 14 nouveaux lauréats de l'appel à projets [Online]. Available: https://presse.ademe.fr/2023/02/ecosystemes-territoriaux-hydrogene-agnes-pannier-runacher-annonce-14-nouveaux-laureats-de-lappel-a-projets.html, . [Accessed 7 March 2023].

[56] Title: status report 2BP Hydrogen buses on the Veluwe Interim report of the deployment of 2 hydrogen buses for passenger transport at Keolis'. 2020.

[57] New bus ReFuelling for European hydrogen bus depots [Online]. Available: www.paulweston.info. [Accessed 27 June 2023].

[58] Huld T, Müller R, Gambardella A. A new solar radiation database for estimating PV performance in Europe and Africa. Sol Energy Jun. 2012;86(6):1803–15. https://doi.org/10.1016/J.SOLENER.2012.03.006.

[59] Hahmann AN, et al. The making of the new European wind Atlas - Part 1: model sensitivity. Geosci Model Dev (GMD) Oct. 2020;13(10):5053–78. https://doi.org/10.5194/GMD-13-5053-2020.
[60] ENTSO-E transparency platform [Online]. Available: https://transparency.entsoe.eu/. [Accessed 21 July 2023].
[61] Haas S, et al. wind-python/windpowerlib. Silent Improvements'; Mar. 2021. https://doi.org/10.5281/ZENODO.4591809.
[62] Oep [Online]. Available: https://openenergy-platform.org/dataedit/view/supply/wind_turbine_library. [Accessed 20 July 2023].
[63] Holmgren WF, Hansen CW, Mikofski MA. 'pvlib python: a python package for modeling solar energy systems'. 2018. https://doi.org/10.21105/joss.00884.
[64] PVGIS typical meteorological year (TMY) generator [Online]. Available: https://joint-research-centre.ec.europa.eu/photovoltaic-geographical-information-system-pvgis/pvgis-tools/pvgis-typical-meteorological-year-tmy-generator_en. [Accessed 21 July 2023].
[65] PV cost and component data - system advisor model - SAM [Online]. Available: https://sam.nrel.gov/photovoltaic/pv-cost-component.html. [Accessed 9 June 2024].
[66] A. Christensen, 'Assessment of hydrogen production costs from electrolysis: United States and Europe'.
[67] IRENA. Renewable power generation costs in 2021. Abu Dhabi, [Online]. Available: www.irena.org; 2022.
[68] Fokkema JE, uit het Broek MAJ, Schrotenboer AH, Land MJ, Van Foreest ND. Seasonal hydrogen storage decisions under constrained electricity distribution capacity. Renew Energy Aug. 2022;195:76–91. https://doi.org/10.1016/J.RENENE.2022.05.170.
[69] Siyal SH, Mentis D, Howells M. Economic analysis of standalone wind-powered hydrogen refueling stations for road transport at selected sites in Sweden. Int J Hydrogen Energy Aug. 2015;40(32):9855–65. https://doi.org/10.1016/j.ijhydene.2015.05.021.
[70] Reddi K, Elgowainy A, Rustagi N, Gupta E. Impact of hydrogen SAE J2601 fueling methods on fueling time of light-duty fuel cell electric vehicles. Int J Hydrogen Energy Jun. 2017;42(26):16675–85. https://doi.org/10.1016/J.IJHYDENE.2017.04.233.
[71] '08358: prices on electricity and grid rent excluding taxes, by consumer group (øre/kWh) 1993 - 2021. Statbank Norway' [Online]. Available: https://www.ssb.no/en/statbank/table/08358/. [Accessed 8 August 2023].
[72] Greenhouse gas emission intensity of electricity generation — European Environment Agency'. Accessed: Aug. 8, 2023. [Online]. Available: https://www.eea.europa.eu/data-and-maps/daviz/co2-emission-intensity-13/#tab-chart_4.
[73] Artigues et Ollières (France) - Parcs éoliens - Accès en ligne - The Wind Power [Online]. Available: https://www.thewindpower.net/windfarm_fr_30929_artigues-et-ollieres.php. [Accessed 6 August 2023].
[74] El puntal (Spain) - wind farms - online access - the wind power [Online]. Available: https://www.thewindpower.net/windfarm_en_15892_el-puntal.php, . [Accessed 6 August 2023].
[75] Lazio 1 (Italy) - wind farms - online access - the wind power [Online]. Available: https://www.thewindpower.net/windfarm_en_36336_lazio-1.php. [Accessed 6 August 2023].
[76] Storheia (Norway) - wind farms - online access - the wind power [Online]. Available: https://www.thewindpower.net/windfarm_en_23747_storheia.php, . [Accessed 6 August 2023].
[77] Giesensdorf (Brandenburg) (Germany) - wind farms - online access - the wind power [Online]. Available: https://www.thewindpower.net/windfarm_en_28738_giesensdorf-(brandenburg).php. [Accessed 6 August 2023].
[78] Boisgibault L. Industrialisation of village in Southern France by solar energy Industrialisation of village in Southern France by solar energy: how energy transition can dynamize a territory? 2014;1. https://doi.org/10.5339/qfarc.2014.
[79] Subsidy-free solar park Don Rodrigo – BayWa r.e. España [Online]. Available: https://www.baywa-re.es/en/solar/solar-park-don-rodrigo#impressions. [Accessed 6 August 2023].
[80] Montalto di castro solar farm - global energy monitor [Online]. Available: https://www.gem.wiki/Montalto_Di_Castro_Solar_Farm, . [Accessed 6 August 2023].
[81] Power plant profile: ASKO midt solar PV plant, Norway [Online]. Available: https://www.power-technology.com/marketdata/power-plant-profile-asko-midt-solar-pv-plant-norway/. [Accessed 6 August 2023].
[82] Senftenberg Joule solar farm - Global Energy Monitor (n.d.). Retrieved August 23, 2024, from, https://www.gem.wiki/Senftenberg_Joule_solar_farm.
[83] Hart E William, Watson J-P, Woodruff DL. Pyomo: modeling and solving mathematical programs in Python. Math Program Comput 2011;3(3):219–60.
[84] Bynum ML, et al. Pyomo — optimization modeling in Python, vol. 67; 2021. https://doi.org/10.1007/978-3-030-68928-5.
[85] Gurobi Optimization L. Gurobi optimizer reference manual. https://www.gurobi.com; 2023.
[86] Oki E. GLPK (GNU linear programming kit)', *linear Programming and Algorithms for communication networks*. Nov. 2012. p. 19–38. https://doi.org/10.1201/B12733-4.
[87] Department for Business Energy and Industrial Strategy (BEIS). 'Hydrogen production costs'. Aug. 2021.
[88] Park J, et al. Green hydrogen to tackle the power curtailment: meteorological data-based capacity factor and techno-economic analysis. Appl Energy Jun. 2023;340:121016. https://doi.org/10.1016/J.APENERGY.2023.121016.